Sandia National Laboratories

Operated for the United States Department of Energy
by National Technology and Engineering Solutions
of Sandia, LLC.
Albuquerque, New Mexico 87185-0747
Livermore, California

date: 18 November 2019

to: Paul E. Shoemaker, 8880
Todd Zeitler, 8863
Ross Kirkes, 8883

from: Rob P. Rechard, 8842
Lawrence C. Sanchez, 8845

subject: Fissile Mass and Concentration Necessary for Criticality in Geologic Media Near Bedded Salt Repository

ABSTRACT

This paper describes the fissile mass and concentration necessary for a critical event to occur in geologic media surrounding the Waste Isolation Pilot Plant (WIPP), an operating repository in southeastern New Mexico for disposing wastes containing transuranic (TRU) radioisotopes from atomic energy defense activities. In the past, concern about criticality in TRU waste has been low because of the low initial concentration of fissile material and the natural tendency of fissile solute to disperse during geologic transport. The potential disposal of TRU waste with high initial concentration of plutonium fissile material prompted a renewed evaluation of the criticality potential. The criticality limits are based on modeling mixtures of fissile plutonium and uranium with water, brine, salt, rust, clay, concrete, sandstone, dolomite, and limestone in an idealized spherical geometry using neutron/photon transport computational codes. In most cases, materials are mixed homogeneously. Geologic media increases the necessary critical mass. Thus, the required critical mass is much larger than pure water mixtures, especially for low enriched uranium. Geologic media can decrease the necessary critical asymptotic concentration to that less than in pure water mixtures when the geologic media is a weak moderator. Understandably, decreasing the geologic porosity increases the critical mass but can cause the critical asymptotic concentration to decrease when the geologic media is a weak moderator. Brine fluids strongly increase both critical limits. Fractured heterogenous media is considered by developing a cell model of planar fractions in regular array to obtain equivalent homogeneous neutron cross-section data. Heterogeneity influences critical mass when the fissile material is confined to fractures in the host rock and the total porosity is small.

I. INTRODUCTION

Like other nuclear facilities, the possibility of sufficient fissile mass and concentration causing a self-sustained neutron chain reaction (criticality) must be evaluated for the Waste Isolation Pilot Plant (WIPP), an operating repository in southeastern New Mexico owned by the US Department of Energy (DOE) for the geologic disposal of wastes containing transuranic (TRU) radioisotopes from atomic energy defense activities (Fig. 1). In the past, concern about criticality occurring in a natural setting from disposal of TRU waste has been low because of the low initial concentration and mass of fissile material (mostly plutonium) in containers and the natural tendency of fissile solute to disperse during transport, as discussed in 2001 and summarized in 2015.[1-3] However, waste destined for WIPP has expanded to include TRU waste with high initial concentration (although still low fissile mass) and /or containers that have larger combined mass limits in the transportation cask.[4] Hence, a renewed evaluation of the likelihood of assembling a critical mass after closure in or near WIPP (e.g., criticality in the Culebra dolomite strata above the repository) has been undertaken for the Compliance Recertification Application for 2019 (CRA-2019).
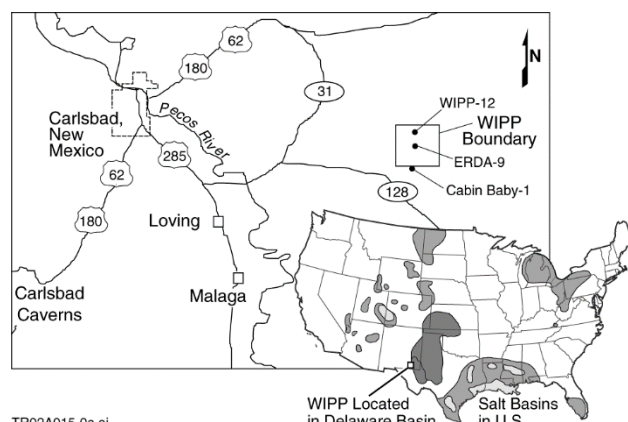
TR02A015-0a.ai

Fig. 1. WIPP repository is 24 km east of Carlsbad in the Delaware Basin in southeastern New Mexico.[1, Fig. 1]

The criticality update for new waste streams is divided into three parts: (1) neutronic criteria necessary for criticality, (2) hydrologic and geochemical causes and constraints on fissile mass deposition,[5] and (3) physical compaction of containers in the disposal rooms through salt creep.[6] This report focuses on the first part, neutronic conditions necessary for criticality to occur sometime in the future after repository closure; thus, the causes of deposition are not important to the discussion here.

Study of the critical scenario in a geologic setting is interesting and instructive because behavior of fissile material differs from common expectations. As a stand-alone article, this memorandum emphasizes this aspect of the critical scenario (hereafter, succinctly referred to as criticality). Yet, using this memorandum in combination with companion memoranda on (a) geochemical constraints on concentrating fissile in various geologic settings,[5] and (b) physical compaction from salt creep and hydrologic[6] demonstrates that the possibility of criticality is remote and not necessary to include in a performance assessment of WIPP.

This memorandum updates previously published calculations for homogeneous spherical configurations in the repository and geologic barrier conducted for the 1996 Compliance Certification Application (CCA-1996) to the US Environmental Protection Agency.[1; 3] Homogeneous mixtures, as discussed in §III, are often more reactive (i.e., neutron flux more effectively utilized) than heterogeneous mixtures, especially at high enrichments of plutonium. However, the reactivity may increase in some configurations of lumped, heterogeneous mixtures of fissile material because the neutrons released in fission can migrate through the rock and water media and miss the large resonances in the non-fissile isotopes of uranium. Consequently, the criticality potential of idealized heterogeneous mixtures, discussed in §VI, is an important addition to the earlier analysis.

The characterization of disposal system and likely depositional waste forms applicable to both the homogeneous and heterogeneous mixtures are discussed below in §II.

II WIPP DISPOSAL SYSTEM

II.A Transuranic Waste

II.A.1 Disposed Fissile Masses

For CRA-2019, the projected combined masses in CH-TRU and RH-TRU of the two most important fissile materials ^{235}U and ^{239}Pu, are 3.0 and 14 metric tons (MT), respectively (Table I). The projected ^{239}Pu enrichment in CH-TRU is 90% for CRA-2019, the same as projected in CCA-1996.

For the criticality calculations herein, the ^{239}Pu enrichment is set at 100%. As seen in Table I, plutonium enrichment will not likely reach 100% ^{239}Pu even though much of the ^{240}Pu and ^{241}Pu throughout the repository would have decayed after 10^3 years. The primary reason for assuming 100% enrichment is that transportation limits use the concept of fissile gram equivalents to convert other radionuclides in contaminated material to ^{239}Pu. The assumed 100% enrichment increases reactivity but not excessively so.

18 November 2019

Table I. Projected fissile material in 2033 for past certifications of WIPP

Radioisotope	CCA-1996[a]		CRA-2004[b]		CRA-2009[c]		CRA-2014[d]		CRA-2019[e]	
	CH (kg)	RH (kg)	CH (kg)	RH (kg)	CH (kg)	RH (kg)	CH (kg)	RH (kg)	CH (kg)	RH (kg)
Uranium										
^{233}U	860	16	130	3.5	16	5.3	10	0.42	11	1.8
^{234}U	75	6.9	45	6.0	49	0.83	34	0.52	77	1.6
^{235}U	5900	2 100	610	440	2 000	33	4 000	31 000	2 100	860
^{238}U	120 000	31 000	73 00	390 000	81 000	880	104 000	88 000	117 000	9 300
Enrichment ^{233}U+^{235}U	4.9%	6.5%	1.0%	0.11%	2.5%	4.1%	3.7%	26%	1.8%	8.4%
Plutonium										
^{238}Pu	15	0.09	73	0.16	86	0.30	35	0.34	55	1.3
^{239}Pu	13 000	170	11 000	87	8 200	47	9 100	120	14 000	68
^{240}Pu	920	22	470	7.5	630	4.4	740	35	1 400	14
^{241}Pu	2.2	0.13	5.0	0.23	4.9	0.04	6.3	0.14	18	0.44
^{242}Pu	310	0.04	6.8	0.12	19	0.32	420	1 600	38	4.0
^{239}Pu fissile kg equivalent[f]	16 700	1 560[g]	11 200	370[g]	9 590	73.0	11 800	20 300[g]	15 500	624[g]
Enrichment ^{239}Pu	90%	88%	95%	92%	92%	90%	88%	6.5%	90%	78%

[a]Ref[7, Appendix BIR Revision 3]

[b]Ref[8]; masses were later updated for EPA requested analysis CRA-2004 PABC

[c]Ref[9]

[d]Ref[10]

[e]Ref[11]

[f]Pu fissile mass equivalence (FME) is the mass of ^{239}Pu plus various factors of the masses of $0.113 \cdot ^{238}$Pu, $0.0225 \cdot ^{240}$Pu, $2.25 \cdot ^{241}$Pu, $0.0075 \cdot ^{242}$Pu, $0.9 \cdot ^{233}$U, $0.643 \cdot ^{235}$U, $0.015 \cdot ^{237}$Np, $0.0187 \cdot ^{241}$Am, $34.6 \cdot ^{242m}$Am, $0.0129 \cdot ^{243}$Am, $15 \cdot ^{245}$Cm, $0.5 \cdot ^{247}$Cm, $45 \cdot ^{245}$Cf, and $90 \cdot ^{251}$Cf.

[g]Pu fissile mass equivalence for RH-TRU derives primarily from $0.643 \cdot ^{235}$U

The projected ^{235}U enrichment of CH-TRU at emplacement for CRA-2019 is 1.8%. The anticipated uranium enrichment at WIPP has remained less than the 4.9% projected in CCA-1996. The anticipated RH-TRU ^{235}U enrichment has varied much more, but the currently projected 8.4% enrichment is similar to the 6.9% enrichment projected in CCA-1996 (Table I).

Based on the WIPP inventory, the uranium enrichment was modeled as 5% or 20% enriched, though an enrichment of 93% was used occasionally to provide a point for interpolating data for intermediate enrichments above 20% for comparison to ^{239}Pu. Uranium and plutonium were considered separately. At low enrichment, uranium behaves as a neutron absorber poison and so neglecting it increases reactivity.

II.A.2. Excess Non-Pit Plutonium

As part of the 1991 Strategic Arms Reduction Treaty (START I) with Russia to dismantle ~80% of strategic nuclear weapons, the US Department of Energy (DOE) identified ~51.7 MT of surplus Pu in various stages of manufacturing at several sites for disposition in a 1996 Programmatic EIS. DOE decided in 2011 to process the ~0.6 MT of miscellaneous Pu and send it to WIPP. In 2012, DOE proposed, and in 2016, DOE selected disposal of the 6.0 MT of non-pit Pu inventory at WIPP and subsequently added it to the WIPP inventory (see Table I, CRA-2019);[4] however it has not yet been shipped. Because bounding estimates were used in CCA-1996, and because estimates for CRA-2004 and thereafter greatly decreased the ^{239}Pu inventory, the disposal of 6.6 MT does not represent an increase in ^{239}Pu over that originally planned in 1996 (Table I).

II.B. Geologic Characteristics of WIPP Disposal System

II.B.1. Castile Formation

The 500-m-thick Castile Formation is the lowest strata discussed here. Within the land-withdrawal boundary of WIPP (Fig. 1), a pressurized brine reservoir was intersected in the fractured Anhydrite III layer of the Castile by one exploratory borehole (WIPP-12) during site characterization (Fig. 2) .[7, Appendix DEL, Section 7.5] Hence, WIPP PAs assume that Castile brine could enter the repository through a new exploratory borehole in the next 10 000 years.

II.B.2. Salado Formation

The 600-m-thick Salado Formation, which overlays the Castile Formation, hosts the WIPP repository 654 m below the surface (Fig. 2). Near the repository, the Salado consists of nearly horizontal (<1° regional dip) rock salt and interbeds of anhydrites and thin clay.[1, Fig. 4] The rock salt is mostly halite with <5%wt dispersed mineral impurities. The impurities, either as intergranular coatings or discrete fine particles, are polyhalite, anhydrite, gypsum, magnesite, various clays, and quartz derived from the clay (Table II).[12] Because of the small amount of mineral impurities in the WIPP rock salt, calculations herein use 100% halite (NaCl).

18 November 2019
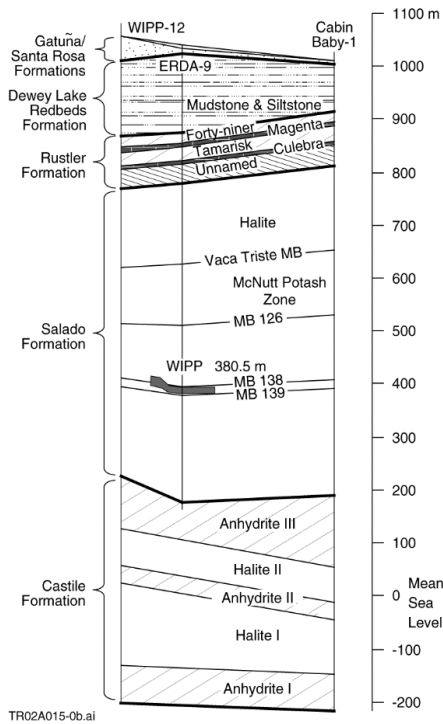
Fig. 2. Stratigraphy near WIPP repository[1, Fig. 4; 13, Fig. 5]

II.B.3. Culebra Dolomite Member of Rustler Formation

The Rustler Formation overlies the Salado. The 7.3-m thick Culebra Dolomite Member of the Rustler Formation, 216 m below the surface, is the most likely pathway for transporting radionuclides away from the repository after an inadvertent human intrusion because it is the most permeable saturated stratigraphic unit (Fig. 2).[13; 14] The Culebra consists mostly of dolomite (85% to 90%) followed by clay (3% to 5%), gypsum, and quartz (Table II).[15, p. 3-9] In three wells, the clay consisted of corrensite (2.25%), illite (1.1%), and minor amounts of serpentine (0.4%), and chlorite (0.16%).[15, Table 3-1] For the criticality

calculations an estimate of the element oxides was used (Table III).[16, Table IV-4]

Table II. Mineralogy of Salado Halite and Culebra Dolomite at WIPP

Mineral (i)	Density (ρ_i) (kg/m^3)	wt %	vol %[a]
Salado Salt			
Halite, NaCl	2165	93.23[b]	94.52
Polyhalite, $K_2Ca_2Mg(SO_4)_4 \cdot 2H_2O$	2775	1.53	1.21
Anhydrite, $CaSO_4$	2970	1.53	1.20
Gypsum, $CaSO_4 \cdot 2H_2O$	2320	1.53	1.45
Magnesite, $MgCO_3$	3009	1.53	1.12
Clay Corrensite	2800	0.64[b]	0.50
Average grain density[c]	2195		
Culebra Dolomite[d]			
Dolomite, $CaMg(CO_3)_2$	2840	91.5	90.71
Clay			
Corrensite $(Ca_{0.6} Na_{0.2} K_{0.2})(Mg_5 Fe_3 Al)$ $(Si_6 Al_2)O_{20} (OH)_{10} \cdot 9H_2O$	2800	2.4	2.41
Illite $(K_{0.6}(H_3O)_{0.4}) (Al_{1.3} Mg_{0.3} Fe_{0.1})$ $S_{3.5} O_{10} (OH)_2 \cdot H_2O$	2750	1.6	1.64
Gypsum, $CaSO_4 \cdot 2H_2O$	2320	3.0	3.64
Quartz, SiO_2	2650	1.5	1.59
Average grain density	2816		

[a] $vol\%(i) = \dfrac{wt\%(i) / \rho_i}{\sum_j wt\%(j) / p_j}$

[b] Halite wt % was measured; silcate residue wt % was measured and here assumed to be corrensite clay; other minerals were set at equal values for the remaining wt % [17, p. 81]

[c] To calculate the bulk density, the porosity varies from 1.8% undisturbed to 5% for reconsolidated salt

[d] Culebra dolomite wt % from Ref[15, p. 3-9]

18 November 2019

Table III. Weight percentages of element oxides associated with WIPP disposal system and related materials

Element Oxides	Culebra Dolomite[b]	Mont-morillinite[c]	NRC Concrete[a]	Pu CCO Mixture[a]	Oklo Sandstone[d]	Yucca Tuff[e,f]	Basalt	Lime-stone
SiO_2	1.55	43.77	72.09	58.50	84.10	74.00	48.50	5.20
CaO	29.39	1.02	6.16		0.02	0.66	8.60	42.64
MgO	21.08			19.80	0.68	0.31	0.83	7.90
Al_2O_3	0.26	18.57	6.42	11.70	7.70	12.40	16.74	0.81
Fe_2O_3	0.22[f]		2.00		2.50	1.07	10.64[f]	0.54
K_2O	0.09				1.84	4.00	1.84	0.33
Na_2O	0.10	1.13	3.91		0.06	3.40	3.53	0.05
TiO_2					0.19	0.10	1.93	0.06
Mn_3O_4					0.02	0.08	0.17	
SO_3	3.30							0.08
P_2O_5						0.01	1.22	0.04
H_2O		36.09	8.94	10.00				0.77
CO2 or 1000°C						1.97	3.79	41.60
Ignition Loss	44.03							
Total	100.00	100.58	99.51	100.00	99.08	99.82	99.00	100.01
Density (ρ^{grain})	2820	2350	2300	2400	2660	2485		2150

[a]Ref[18, App. A]

[b]Ref[16, Table IV-4]; WIPP-12 at 246.7 m depth (Fig. 1)

[c]webmineral.com accessed 12-5-18; based on *Eur. J. Min.* **9**:821-827 (1997); composition based on empirical formula

[d]Ref[19, Table 3]; near natural reactors where not much silica has dissolved and where < 0.10% UO_2

[e]Average of values for Tptpmn, Tptpll, and Tptpln stratigraphic modeling units[20, App. A]; Similar composition in Ref[21]

[f]Reported as FeO

The Culebra has been divided into four units near the WIPP repository (Fig. 3).[2, Fig. 5 22] The uppermost unit, Culebra Unit 1, averages 3.0 m in thickness but is not transmissive with only a small number of large-scale discontinuous fractures that occur along bedding planes, and some microvugs. Originally, vugs were anhydrite pockets that hydrated to gypsum during sedimentation; subsequent dissolution of gypsum left the vugs.

The middle Culebra Units, 2 and 3, are similar with small-scale fracturing. Culebra Unit 2 is about 1.6 m thick; Culebra Unit 3 is about 1.2 m thick. Because of more extensive fracturing, intact pieces of core from Culebra Unit 3 are rare. The fractures in both units are either open or gypsum-filled, with apertures up to 2 mm wide. Micro (< 0.05 m long and spaced 1 to 10 cm) and randomly oriented fractures (0.05 m to 0.2 m long and spaced 2 to 20 cm) are abundant. Subvertical fractures (0.2 to 1 m long and spaced <50 cm apart) and bedding plane fractures (< 1 m long and spaced 5 cm to 40 cm) are common. The fractures connect abundant microvugs (< 3 mm in diameter) and some large vugs (0.3 cm to 10 cm in diameter).

The total (or bulk) porosity of the Culebra Dolomite Member of the Rustler is the sum of the vug ($\bar{\varphi}^{vugs}$), fracture ($\bar{\varphi}^{frac}$), and matrix porosities ($\bar{\varphi}_{Culebra}^{matrix}$), that is

$$\phi_{Culebra}^{total} = \bar{\varphi}^{vugs} + \bar{\varphi}^{frac} + \bar{\varphi}_{Culebra}^{matrix}(1 - \bar{\varphi}^{vugs} - \bar{\varphi}^{frac}) \quad (1)$$
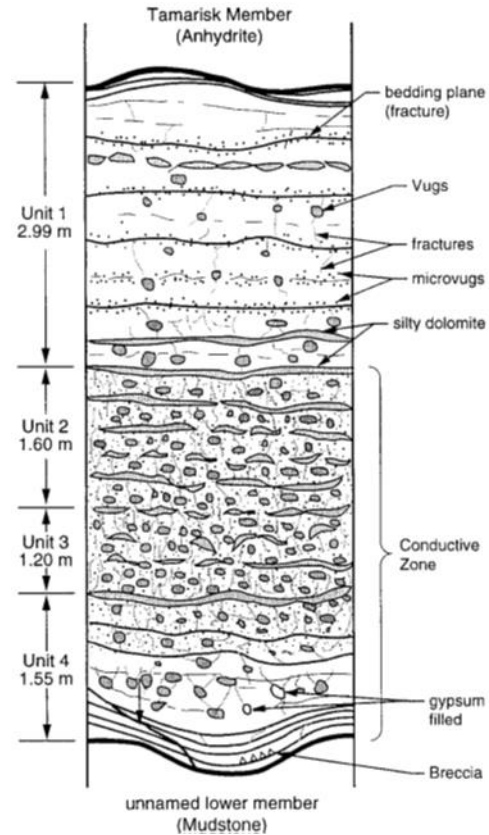
Fig. 3. Stratigraphic divisions of Culebra Dolomite Member of Rustler Formation.[23, Figure 3-6]

18 November 2019

The micro-vug porosity $\overline{\varphi}^{vugs}$ of the lower 3 units is fixed at 0.05. Based on tracer tests in 1996, the advective fracture porosity $\overline{\varphi}^{frac}$ of the lower 3 units is loguniformly distributed between 10^{-4} and 10^{-2} with a median of 10^{-3}.[24, Fig. 23] An advective porosity of 4×10^{-2} was also used and is used here as a bounding value. In WIPP PAs, the fracture spacing (2B) is loguniformly distributed between 10 and 100 cm,[24, Fig. 24] but smaller values between 1 to 5 cm, corresponding to the microfractures in Units 2 and 3, are often used here. The intact matrix porosity $\overline{\varphi}_{Culebra}^{matrix}$ is distributed between 0.10 and 0.25 with a median of 0.16. [22; 25, Fig. 2.-10 & Table 2.6-3]

Table IV. Total porosity of Culebra dolomite for various fracture, vug, and matrix porosities

Vugs $\overline{\varphi}^{vugs}$ (%)	Fracture $\overline{\varphi}^{frac}$ (%)	Matrix $\overline{\varphi}_{Culebra}^{matrix}$ (%)	Equivalent Matrix and Vugs (%)	Total $\phi_{Culebra}^{total}$ (%)
5	4.0	10	15	18
		16	20	23
		21	25	28
		25	29	32
	1.0	10	15	15
		16	20	21
		21	25	26
		25	29	30
	0.1	10	15	15
		16	20	20
		21	25	25
		25	29	29

II.B.4. Brine Compositions for Criticality Calculations

In the criticality calculations, the composition of the Castile brine is from exploratory borehole ERDA-6 (Table V).[17; 26] The WIPP rock salt contains a small amount of interstitial Salado brine not bound in hydrous minerals or fluid inclusions (~0.3%wt in clear halite, ~1.5%wt in argillaceous salt, and ~2.2%wt in clay seams).[27] The Salado brine, as measured at the repository horizon in the experimental Room Q, has substantially more magnesium, potassium, chloride, and boron than Castile brine, where the Cl^{-1} concentration of 5100 mM and B^{+3} concentration of 144 mM are particularly important for criticality analysis. The brine in the Culebra dolomite, as measured in the Air Intake Shaft, is only slightly more saline than brackish water.[a]

Table V. Composition of Castile, Salado, and Culebra brines near WIPP.[17]

Constituent	Brine Concentration (mM or mole/m³)		
	Culebra (Air Intake Shaft)	Salado (G - Seep)	Castile (ERDA - 6)
Sodium (Na^{+1})	600	4110	4870
Magnesium (Mg^{+2})	21	630	19
Potassium	8.3	350	97
Calcium (Ca^{+2})	23	7.68	12
Boron (B^{+3})	2.8	144	63
Chloride (Cl^{-1})	567	5100	4800
Sulfate (SO_4^{-2})	77	303	170
Bromine (Br^{-1})	0.37	17.1	11
Bicarbonate (HCO_x^{-1})	1.1	0.01	16
Ionic strength	800	6700	5300
Total dissolved solids (kg/m³)			
Calculated	43.2	337	305
Measured	42.6	355	330
Specific Gravity	1.040	1.230	1.216
pH	7.70	6.10	6.17

III. CALCULATION OF CRITICAL CONCENTRATION AND MASS FOR HOMOGENEOUS SPHERE

A critical condition depends not only on the quantity of fissile material but also on its concentration, shape, and any other material mixed with or surrounding the fissile material. Setting limits for a heterogeneous mixture with specific shapes and masses of fissile and other material is complex. However, limits below which criticality is impossible can be calculated for homogeneous mixtures of fissile material in a spherical shape, and these bounding limits can provide guidance in more complex situations.

III.A. Computational Tools

III.A.1 SCALE

Although numerous criticality experiments have been performed in ideal material and fuel assemblies in reactors, criticality experiments with common geologic material have not. Consequently, two computational tools are used to estimate limits. Most models were developed with the SCALE v6.1 modular code system for neutron and photon transport using the 238 group Evaluated Nuclear Data File/B Version 7.1 (ENDF/B-VII.1) criticality library of tabulated cross-sections, which is provided in the standard release of SCALE (and MCNP). Within SCALE, the XSDRN module was used, which deterministically solves the one-dimensional Boltzmann transport equation in spherical coordinates. XSDRN has been used for almost four decades and particularly useful here because of its flexible search capability. The convergence criterion in XSDRN was set at a relative accuracy of 10^{-3}.

In the SCALE model, a spherical core of fissile material and fluid in the pores of the geologic material is

---

[a]Brine refers to an aqueous solution with total dissolved solids (TDS) greater than 30 kg/m³. For comparison, brackish water refers to solutions with TDS between 3 and 30 kg/m³. Sea water has TDS of ~35 kg/m³ and fresh water has TDS < 3 kg/m³.

18 November 2019

surrounded by a spherical reflector with a radius 2 m greater than the core to approximate a reflector of infinite extent ($r^{core}+2m$). The spherical reflector has the same composition as the spherical core, but the fissile component in the porosity is replaced with additional fluid (either water or brine).

To estimate a point on the curve describing the relationship between fissile concentration and fissile mass, calculations start by solving for $k^{\infty}=1$ to find the fissile minimum critical concentration for a core of infinite extent (theoretically found by setting the divergence in the Boltzman transport equation to zero, but usually implemented by setting a perfect reflecting boundary condition). Next, a rough estimate of the diameter of spherical core of finite extent is made. Finally, the core-plus-reflector sphere is then expanded (or contracted) until XSDRN finds a critical diameter and corresponding minimum fissile mass at $k^{eff}=1$.

Five parameters describe the homogeneous model (and are common to the heterogeneous model described in §VI): (1) void fraction not occupied by geologic material (matrix porosity in Table IV), (2) fraction of the void that is occupied by fissile material ($0< f_{matrix}^{fissile} <1.0$), (3) enrichment of fissile material, (4) grain density of mineral form of fissile material (ρ^{grain}), and (5) type of fluid filling pores, where

$$\rho_{bulk}^{fissile} = \rho^{fissile}(\phi^{matrix} f_{matrix}^{fissile}) \qquad (2)$$

$$\rho_{bulk}^{fluid} = \rho^{fluid}[\phi^{matrix}(1- f_{matrix}^{fissile})] \qquad (3)$$

$$\rho_{bulk}^{rock} = \rho^{rock}(1-\phi^{matrix}) \qquad (4)$$

where $\rho^{fissile}$, ρ^{rock}, and ρ^{fluid} are the depositional density of the fissile mineral, rock gain density, and fluid density, respectively, and ϕ^{matrix} is the matrix porosity of the intact rock.

III.A.2 MCNP

Several models were also developed with MCNP™ (Monte Carlo code for solving Neutron and Photon transport equations) (Version 6.2) to compare results.[28] In MCNP, the integral neutron and photon transport equations are solved with Monte Carlo techniques. The distance between interactions, the fissions that occur, the loss by capture, or leakage are characterized by parameters such as the reaction cross-section of the atoms of each material, the mean free path lengths between interactions, the distribution describing scattering, and the distribution of neutron energy. The relative fractional error on the eigenvalue was 2.0×10^{-4} on all MCNP results.

III.B. Critical Limit and Bias

A system is "critical" when a nuclear chain reaction is sustained, which is mathematically expressed by a neutron multiplication factor (k) of unity, where k is defined as the number of neutrons in one generation divided by the number of neutrons in the preceding generation for the entire fissile system or assembly (i.e., integrated over the entire system). Traditionally, k^{eff} denotes a multiplication factor for a system of finite extent, and k^{∞} denotes the multiplication factor for a homogenous system of infinite extent.[29, pp. 75-84]

The limit for when a fissile configuration is considered critical is derived from the bias and uncertainties associated with the criticality code (SCALE or MCNP), the underlying nuclear data, and the modeling fidelity. In an engineered system on the surface with humans present, great care is taken to conservatively define the most appropriate limit to prevent criticality (i.e., critical limit = k^{eff} – (calculational bias + uncertainties)). In geologic systems, however, factors such as variation in the porosity, saturation, and host rock composition have much more influence on the minimum masses and concentrations than calculational biases and uncertainties in k^{eff}.

More importantly, the critical limit varies by mineral form and is non-linear at low enrichments (e.g., for Rutherfordine—UO_2CO_3, the conservatism of a critical limit between 1.0 and 0.96 at 3% enriched is large compared to that at 93% enriched—Fig. 4). Hence, we assume the critical limit is k^{eff} and that we are subcritical when $k^{eff} < 1.0$ throughout the article to be consistent between enrichments and mineral forms.
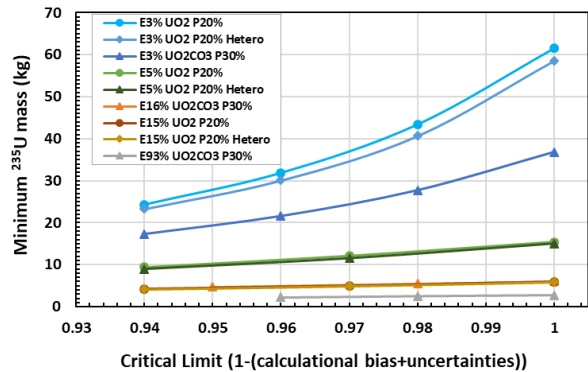
Fig. 4. Critical-limit criteria on critical mass for ^{235}U as uraninite and Rutherfordine in Culebra dolomite is non-linear at low enrichment.

III.C. Critical Limits for Fissile-Fluid Mixtures

Homogeneous fissile/fluid mixtures provide convenient bounds on minimum mass and minimum concentration required when developing the rationale for screening out the possibility of criticality after WIPP closure.

Based on calculations for ^{239}Pu in infinite mixture with k^{eff} of unity, the minimum ^{239}Pu mass is 0.51 kg at a concentration of 32 kg/m^3. The ^{239}Pu mass must exceed 0.51 kg for criticality to occur at any concentration of 100% enriched ^{239}Pu in pure water mixture (Fig. 5). For

this ^{239}Pu/H$_2$O mixture, the calculated criticality curve compares quite well with compiled experiments (Fig. 5).[30; 31]

As the water amount decreases such that the ^{239}Pu concentration increases beyond 32 kg/m^3 at the minimum mass, the system becomes under moderated and the concentration of 100% enriched ^{239}Pu approaches the ^{239}Pu metal density of 19 840 kg/m^3 at a mass of ~6 kg. The system is under moderated because enough moderating material (here water) is not available to sufficiently slow down many of the neutrons and thereby be captured by the ^{239}Pu fissile nucleus. Hence, the necessary mass of ^{239}Pu for the system to reach a k^{eff} of unity must increase significantly from the minimum critical mass.

As the ^{239}Pu concentration decreases from 32 kg/m^3 through the addition of water, the system becomes over moderated. The necessary ^{239}Pu mass for criticality increases exponentially as the ^{239}Pu concentration asymptotically approaches 7.2 kg/m^3 where k^{∞} is unity.

Criticality is impossible at ^{239}Pu concentrations less than 7.2 kg/m$^{3.}$

The minimum critical Pu concentration is much larger in brine from the Salado and Castile Formations (Fig. 2): a factor of 7 and 5.5 larger than water (50 kg/m^3 and 40 kg/m^3, respectively). The minimum mass is a factor of 10.5 and 7 larger than water (5.5 and 3.7 kg, respectively—Table VI). Hence, criticality is unlikely when Castile or Salado brine has entered the WIPP disposal region.

The corresponding critical spherical radius at the critical concentration and mass is practically identical in water and dilute Culebra brine (0.15 m) and similar in Salado and Castile brines (0.18 m and 0.19 m). Although the necessary fissile spherical radius plateaus somewhat around 300 kg/m^3, the sphere radius continues to decrease monotonically to 0.04 m as the concentration increases to the ^{239}Pu metal density.
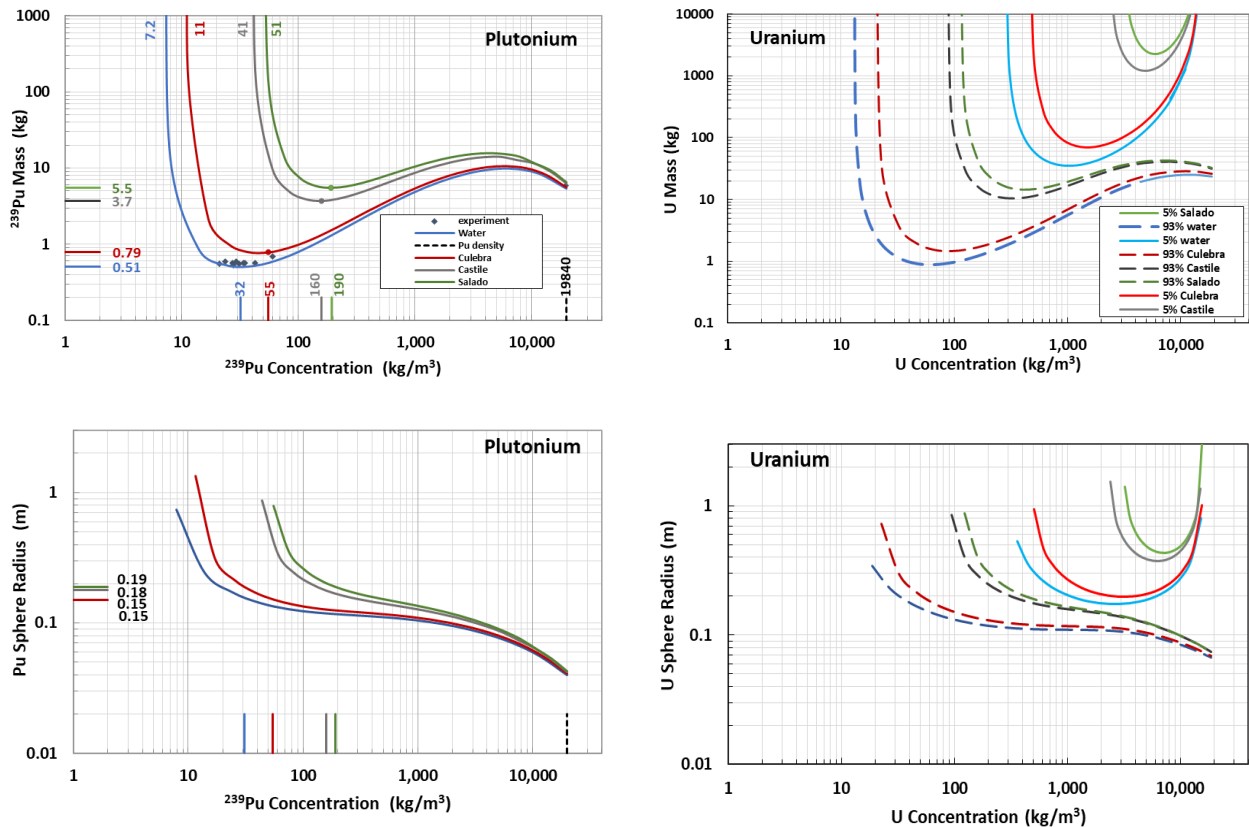
Fig. 5. Calculated and measured critical mass and radius as function of fissile concentration in a homogeneous, spherical shape in water and WIPP brines:[1, Fig. 5; 30; 31; 32, Fig. 7] (a) 100% enriched plutonium mass, (b) 5% and 93% enriched uranium, (c) plutonium radius, and (d) uranium radius.

Table VI. Minimum concentration for infinite mixture and minimum mass and concentration for reflected sphere of plutonium and uranium mixed homogeneously with WIPP brines and salt, goethite, concrete, or Culebra dolomite materials at 20% total porosity as calculated by SCALE and MCNP.

Fluid	Solid Material at 20% Porosity	SCALE Infinite Mixture Min Concen (kg/m^3)	SCALE Reflected Sphere Mass Min (kg)	SCALE Reflected Sphere Radius Min (m)	SCALE Reflected Sphere Conc at Min Mass	MCNP[a] Infinite Mixture Min Concen (kg/m^3)	MCNP[a] Reflected Sphere Mass Min (kg)	MCNP[a] Reflected Sphere Radius Min (m)	MCNP[a] Reflected Sphere Conc at Min Mass
Plutonium 100% enriched									
Water	none	7.22	0.521	0.143	42.5	7.23	0.505	0.156	31.9
	Goethite (FeO(OH))	19.1	2.97	0.218	68.6	18.5	2.98	0.218	79.0
	Culebra Dolomite	3.06	1.61	0.294	15.1	2.89	1.81	0.314	14.0
Salado	none	51.2	5.47	0.190	192	51.7	5.33	0.189	189
	Salt (NaCl)	186	129	0.247	2042	233	124	0.244	2030
	Goethite	26.3	4.81	0.231	93.1	26.8	4.81	0.226	99.5
	NRC Concrete	13.2	6.47	0.316	49.1	13.3	5.95	0.306	49.1
Castile	none	41.0	3.69	0.180	158	40.4	3.83	0.180	158
	Goethite	25.5	4.23	0.230	83.4	24.7	4.33	0.226	89.2
Culebra	none	11.2	0.789	0.150	55.3	11.2	0.799	0.152	54.1
	Culebra Dolomite	3.73	2.07	0.320	15.1	3.68	2.32	0.3324	15.1
Uranium 15% enriched									
Water	none	~88.0	7.45	0.172	351	Not Calculated	7.18	0.165	380
Uranium 5% enriched									
Water	none	291	35.1	0.202	1020	Not Calculated	32.0	0.194	1070

[a]See Appendix A

SCALE and MCNP values for Pu minimum critical concentration for water and WIPP brines agree to within 1.5% (Table VI and Table VII). The Pu minimum critical masses agree to within 3%. The values are not entirely comparable in that SCALE values are minimums found when linearly spacing out points, not the results of a systematic search. On the other hand, MCNP values are the result of a manual search for minimums starting with the SCALE values. When reporting minimums in the text, MCNP values are usually used.

For criticality to occur in a 93% enriched U/H$_2$O mixture, the ^{235}U mass and solid concentration must be > 0.87 kg and >13 kg/m^3, respectively. For criticality to occur in a 5% enriched U/H$_2$O mixture, the ^{235}U mass and solid concentration must be >36 kg and >300 kg/m^3, respectively (Fig. 5). The critical mass and concentration increase substantially in WIPP brines.

For 5% enriched uranium with either too much water (i.e, over moderated with uranium concentration near 290 kg/m^3 at k^∞) or very little fluid (i.e., under moderated with uranium concentration near 19 050 kg/m^3), the total mass of uranium must increase exponentially because enough water is not present to moderate neutrons sufficiently to be captured by the nucleus of the small amount of ^{235}U present.

Table VII. Percent difference between MCNP and SCALE calculated critical limits for Pu and U

Fluid	Solid Material at 20% Porosity	SCALE and MCNP Differences[a] Infinite Mixture Min Conc (%)	SCALE and MCNP Differences[a] Reflected Sphere Mass Min (%)	SCALE and MCNP Differences[a] Reflected Sphere Radius Min (%)	SCALE and MCNP Differences[a] Reflected Sphere Conc at Min Mass
Plutonium 100% enriched					
Water	none	-0.1	3.2	-8.3	33.2
	Goethite (FeO(OH))	3.2	-0.3	0	-13.2
	Culebra Dolomite	5.9	-11.0	-6.4	7.9
Salado	none	-1.0	2.6	0.5	1.6
	Salt (NaCl)	-20.2	4.0	1.2	0.6
	Goethite	-1.9	0	2.2	-6.4
	NRC Concrete	-0.8	8.7	3.3	0
Castile	none	1.5	-3.7	0.6	0
	Goethite	3.2	-2.3	1.8	-6.5
Culebra	none	0	-1.2	-1.3	2.2
	Culebra Dolomite	1.4	-10.8	-3.6	0
Uranium 15% enriched					
gWater	None		3.8	4.2	-7.6
Uranium 5% enriched					
Water	none		9.7	3.9	-4.7

[a] Difference from MCNP calculated estimate

18 November 2019

Similar to high enriched Pu, a minimum radius does not occur for highly enriched U. For low enriched U, however, a minimum radius does occur that provides a geometric constraint at the required space for deposition (Fig. 5).

When expressed as ^{235}U rather than U, the minimum critical concentration range in water is quite narrow; the solid concentration must be >16.5 kg for 3% enriched uranium >12 kg/m^3 for 93% enriched and (Fig. 6). Thus, the minimum critical concentration decreases as ^{235}U enrichment increases. The minimum concentration also decreases as ^{239}Pu enrichment increases but the percentage change is greater for brines than for water (Fig. 7)
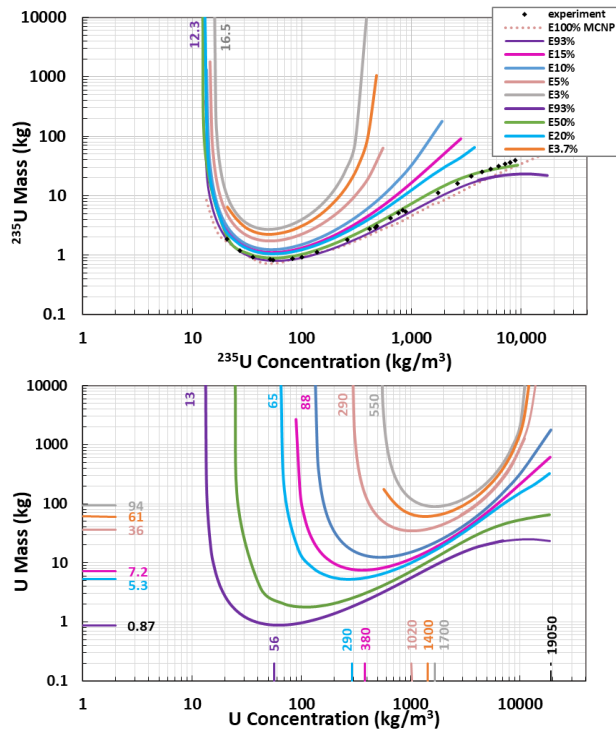
Fig. 6. Uranium calculated and measured critical concentration at various enrichments in a homogeneous, spherical shape in water:[1, Fig. 5; 30; 31; 32, Fig. 7](a) ^{235}U, and (b) total uranium.
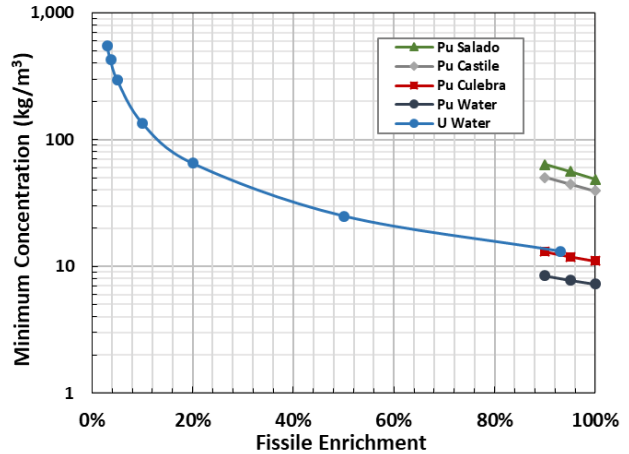
Fig. 7. Decrease of minimum critical concentration with increase in ^{239}Pu enrichment in WIPP brines.

III.D. Minor Influence of Deposited Mineral at High Enrichment

III.D.1. Mineral Form of Plutonium

Plutonium is usually modelled as pure uncombined ^{239}Pu when it is mixed with fluids (as brines §III.C above), adsorbed on clay (as montmorillonite §IV.A below), or adsorbed on rust (as goethite §IV.B below).

Elsewhere, plutonium deposited in either the repository or the geologic barrier is usually modeled as plutonium dioxide (PuO$_2$ with ρ_g = 11 582 kg/m^3 and 88% of density as Pu^{IV}), rather than modeled with water of hydration or hydroxyl groups (i.e., PuO$_2$(OH)$_2$ • H$_2$O or Pu(OH)$_4$). The mineral form influences criticality limits for highly enriched ^{239}Pu only when the mixture is highly under moderated (Fig. 8a). The bound hydrogen in Pu minerals, such as PuO$_2$(OH)$_2$ • H$_2$O or Pu(OH)$_4$, increases reactivity in fairly dry configurations, but the neutronic influence of the bound hydrogen on reactivity is overwhelmed by aqueous water in most saturated configurations.

Additional materials within or released from the TRU container, including neutron poisons and fission products, were neglected in the analysis here. Neglecting fission products and neutron poisons is very conservative but to determine how conservative would require significant effort to model the transport of all chemical species and is beyond the scope of this memorandum.

18 November 2019
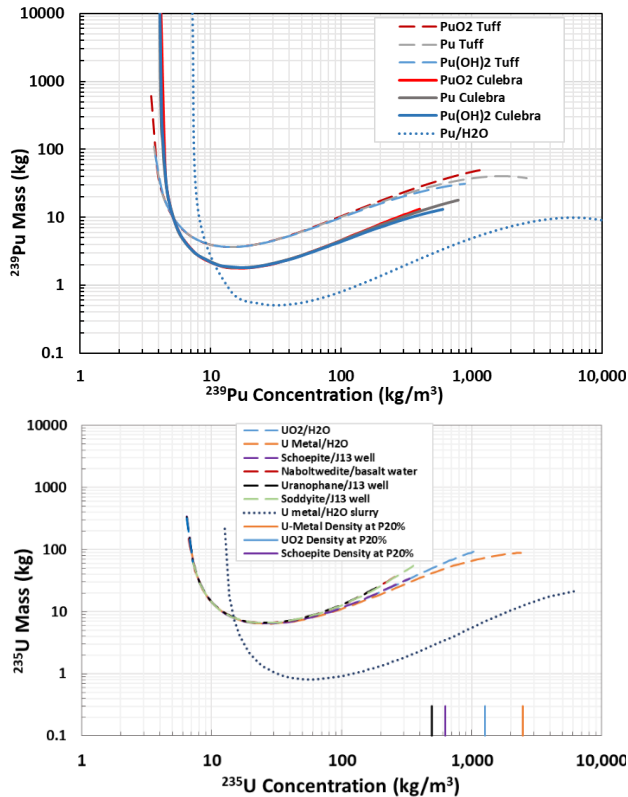
Fig. 8. Mineral forms of highly enriched fissile material have little influence on the critical limits except when highly under moderated (a) 100% enriched ^{239}Pu in Culebra dolomite or volcanic tuff, and (b) 93% enriched ^{235}U in volcanic tuff.

III.E.2. Mineral Forms of Uranium

Uranium is modeled as pure uncombined ^{235}U when uranium is mixed with fluids and adsorbed on clay or rust. Deposited uranium is modeled as uranium dioxide in the repository and the geologic barrier of the disposal system (UO$_2$ with ρ_g = 10 970 kg/m^3 and U^{IV} 88% of density). Uranium dioxide corresponds to the manufactured form of the fuel. Granted, uraninite is the depositional form that would occur in reducing regions of the disposal system, but the density change is minor (UO$_2$ with natural density of 10 600 kg/m^3).

Uranium deposition in the dolomite, above the WIPP repository, is also modeled as Rutherfordine (UO$_2$CO$_3$ with ρ_g = 5724 kg/m^3 and U^{VI} 72%wt of density) because it is the thermodynamically stable form for U^{VI} in a carbonate solution. Like Pu, depositional forms of highly enriched ^{235}U in Culebra dolomite have little influence on critical limits except when highly under moderated (Fig. 8b).

III.E. Influence of Deposited Uranium Minerals at Low Enrichment

The mineral form of the uranium influences the critical limits at the enrichments <20% (Fig. 9).

However, the influence is rather small for the two potential depositional minerals encountered in the Culebra dolomite of the WIPP disposal system: either UO$_2$ or Rutherfordine—UO$_2$CO$_3$. Nonetheless, critical limits for both mineral forms are frequently evaluated.
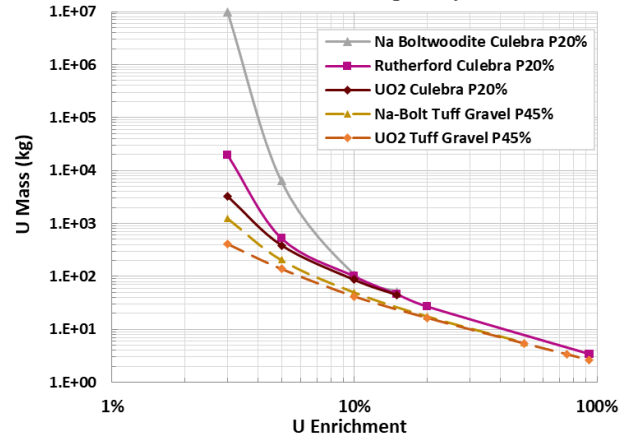
Fig. 9. Uranium mineral form only important when enrichment <20% in Culebra dolomite at 20% porosity or tuff gravel at 45% porosity.

IV. CRITICAL LIMITS FOR FISSILE HOMOGENEOUS SPHERE IN VARIOUS MATERIALS

Except for well hydrated material such as the montmorillonite clay discussed first, the addition of geologic media to a fissile/water binary system substantially increases the mass of fissile material necessary to go critical for both ^{239}Pu and ^{235}U.

IV.A. Fissile Critical Limits in Hydrated Clay

Fissile material can adsorb on clays naturally present in fine layers of the Salado Formation and Culebra dolomite. In addition, bentonite clay, composed mostly of montmorillonite, is a likely engineered material to use in closing shafts and known boreholes within the WIPP disposal system (Table III).

Montmorillonite is composed of three basic structural layers: a silicate sheet of silicon tetrahedron units (Si$_4$O$_{10}$) sandwiched between gibbsite sheets of aluminum octahedron units (Al$_2$(OH)$_6$), in which two out of every three (OH) ions are replaced with an oxygen of Si$_4$O$_{10}$ (i.e., Al$_2$(OH)$_2$). For montmorillonite, some isomorphous substitution of Al^{+3} with Mg^{+2} has occurred within the gibbsite sheets.[33, p. 46] The charge imbalance from the substitution is compensated by the presence of interlayer Na^{+1} and Ca^{+2} cations. Water (H$_2$O) molecules are readily absorbed in the interlayers between the montmorillonite structural groups. The clay greatly expands and contracts as water is absorbed by wetting and removed by drying. When Ca^{+2} is the interlayer cation (most common), often two layers of water molecules are present; when Na^{+1} is the interlayer cation,

18 November 2019

between one and three water molecule layers are present.[34, p. 264]

Montmorillonite has the general chemical formula $(Na,Ca)_{0.3}(Al,Mg)_2Si_4O_{10}(OH)_2 \cdot nH_2O$ with density between 2000 and 2700 kg/m^3. Here we use a well hydrated composition of $Na_{0.2}Ca_{0.1}Al_2Si_4O_{10}OH_2 \cdot 10H_2O$ with density of 2350 kg/m^3 and molecular weight of 549.07 g/mol. Because of the high-water content in the clay (water of hydration is 10 H_2O), well hydrated clay with fissile material behaves like a binary mixture of Pu/water. Thus, the porosity of the clay is immaterial for evaluating neutronic criteria (Fig. 10).

When the porosity is filled with either Castile or Salado brine the behavior is not identical to a Castile or Salado binary system because of the water of hydration in the clay, and instead the behavior is in between water and brine binary systems, and porosity has some influence.

In reality, however, a mixture of clay with brine is more complicated. The addition of brine actually dehydrates the clay (perhaps by 25%), which would move the curve closer to the Pu/brine system than shown. Yet, dehydration also decreases the porosity and so less brine would be in the system, which would move the curve back toward the Pu/water system. Hence, the actual position of the criticality curve for a Pu/clay/brine system is somewhat uncertain because of the competing influences.
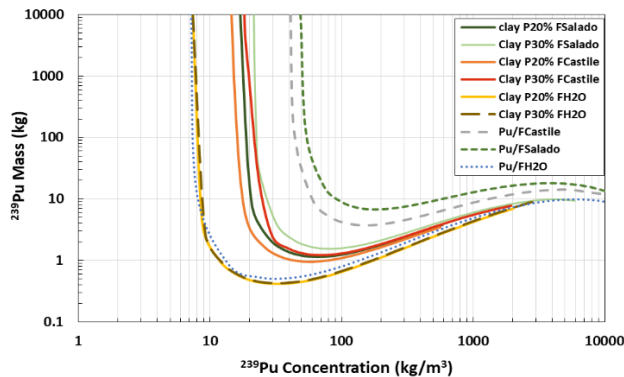
Fig. 10. Fissile ^{239}Pu/montmorillonite clay at 20% to 30% porosity saturated water and WAPP brine.

IV.B. Fissile Critical Limits in WIPP Salt

As noted in §III.C, the minimum critical concentration in Salado brine is a factor of 7 larger than in water because of the neutron adsorption by Cl⁻. The addition of salt matrix increases the minimum critical concentration further (Table VI). The critical mass concentration reaches a maximum of ~186 kg/m^3 (~9.3%wt in dry Halite) for 100% enriched PuO_2 in Halite at between 15% and 20% porosity saturated with Salado brine (which is an additional factor of 3.6 or factor of 26 beyond water) (Fig. 11).
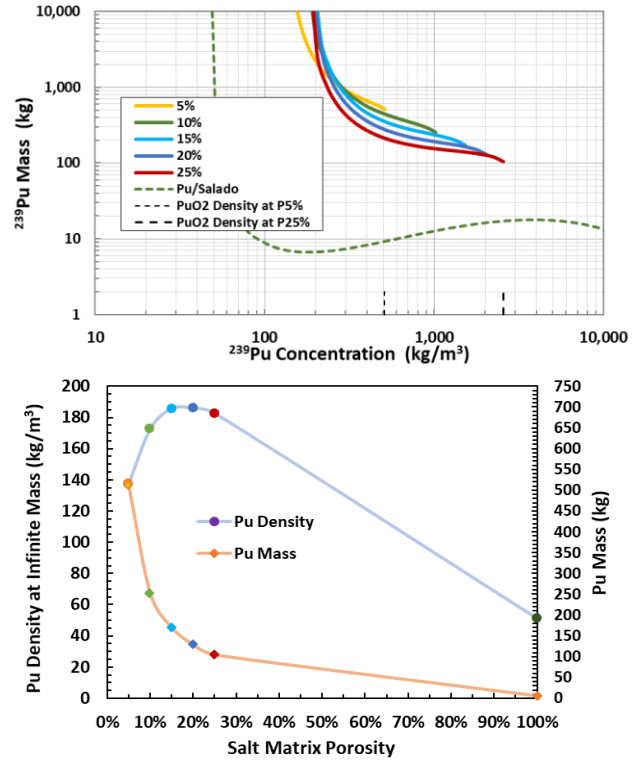
Fig. 11. Critical limits for PuO_2 100% enriched in ^{239}Pu in Halite saturated with Salado brine (a) Critical minimum mass when porosity filled, (b) Largest critical concentration 186 kg/m^3 (~9.3%wt) between 15% and 20% matrix porosity

As the salt matrix porosity increases beyond 20%, the critical concentration decreases to that of brine (i.e., as porosity increases in a strong absorbing media, the critical concentration decreases.

As the porosity decreases below 15%, however, the critical concentration also decreases somewhat because of loss of moderating hydrogen in the brine. For 10% and 5% porosity, the critical concentration is 173 kg/m^3 (~8.3%wt in dry Halite) and 138 kg/m^3 (~6.4%wt in dry Halite), respectively (Fig. 11).

The addition of salt matrix greatly increases the minimum critical mass. Because of the small matrix porosity available in salt, the minimum critical mass occurs when fissile ^{239}Pu completely fills the Halite porosity (e.g., the minimum critical mass at 25% porosity occurs when the critical Pu concentration is at the density of PuO_2 with porosity 25%).

Although not shown, the minimum critical mass in salt would decrease somewhat for pure Pu mineral because more ^{239}Pu can reside in the limited salt porosity for pure Pu with smaller volume than PuO_2. This situation is like the situation observed earlier for a binary fissile/fluid mixture, where the Pu mineral form with high density influenced the minimum mass when the system was severely under moderated (Fig. 8). In a

18 November 2019

fissile/salt/brine mixture, the system quickly becomes under moderated because of the limited salt porosity.

The minimum critical mass for PuO_2 varies between 510 kg at 5% porosity and 100 kg at 25% porosity (Fig. 11). As the porosity continues to increase the 100-kg ^{239}Pu critical mass at 25% porosity eventually decreases a factor of 19 to a minimum mass of 5.5 kg in ^{239}Pu and Salado brine (Fig. 5 and Table VI).Although uranium disposed in CH-TRU at WIPP is ~1.8% enriched in ^{235}U (or ~2.3% for CH- and RH-TRU combined—Table I), an enrichment of 20% was used here to display the critical limits because of the extreme high mass and critical concentration at smaller enrichments. The critical concentration is 180 kg $^{235}U/m^3$ (6.3%wt) at 10% porosity and 283 kg $^{235}U/m^3$ (8.6%wt) at 20% porosity for 20% enriched UO_2 (Fig. 12). The critical minimum mass of 28 000 kg ^{235}U, which occurs when U completely fills the halite porosity, is only slightly less than the 29 570 kg currently planned to be disposed at WIPP, including 25% decay of ^{239}Pu over 10^4 years (i.e., 2570 kg ^{235}U + 0.25(12 000 kg ^{239}Pu)—Table I).
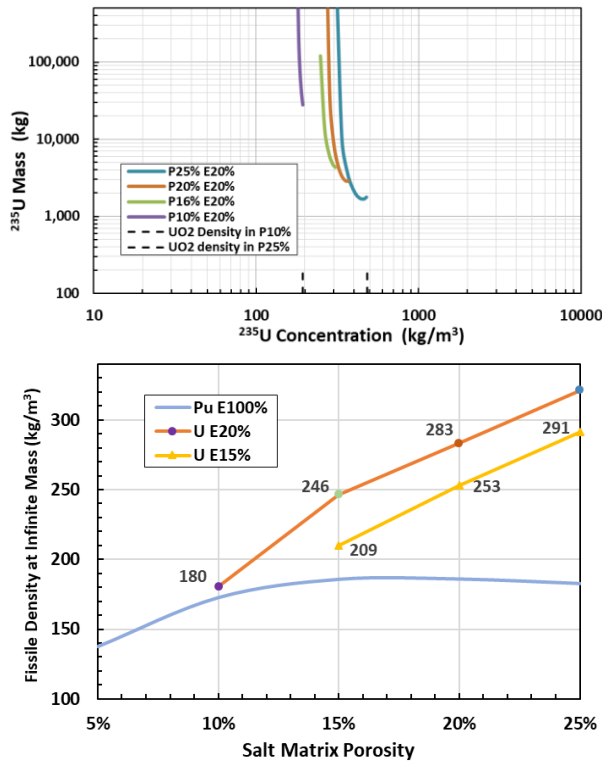
Fig. 12. Critical limits for 15% and 20% enriched UO_2 in salt saturated with Salado brine (a) Critical minimum mass when porosity filled, (b) concentration is 283 kg /m^3 at 20% porosity for 20% enriched uranium.

IV.C. Fissile Critical Limits in Iron

Fissile material can adsorb onto corrosion products of the drums and metals in the waste within the repository, most notably iron corrosion products. If the WIPP repository is somewhat oxidizing, the initial iron corrosion products of the steel may be particles of amorphous ferrihydrite (i.e., Fe^{+3}). Amorphous ferrihydrite (nominally am-$5Fe_2O_3 \cdot 9H_2O$ though the formula varies with water content) may progress, through dehydration and aggregation, to more crystalline iron oxides, provided metal cations readily absorbed do not block the transformation.[35] Ferrihydrite is rapidly catalyzed by Fe^{+2} to form goethite (α-FeO(OH)), lepidocrocite (γ-FeO(OH)—a polymorph with different crystal structure favored in chloride solutions), or magnetite ($Fe^{+2}Fe_2^{+3}O_4^{-2}$).[36] Transformation of ferrihydrite to hematite (Fe_2O_3) can take longer.

Because the formula for ferrihydrite is indeterminate and formation of hematite can be lengthy, we assume goethite is the primary iron corrosion product at WIPP and evaluate critical limits for homogeneous mixtures of goethite with Pu and U ions through adsorption. The porosity of iron oxides varies widely, and we use a porosity of 20%.

In a mixture of Pu with goethite, the critical concentration and mass are greatly increased from that of Pu mixed solely with water because of neutron adsorption by Fe (when some hydrogen is present to moderate the neutrons). The critical concentration of a Pu/goethite/water mixture is 19 kg/m^3 (0.79%wt), as used previously for CCA-1996.[1, Fig. 10]

Although the critical concentration and mass increases further when the fluid is brine, the type of brine (either Castile or Salado) does not matter much (e.g., the critical concentration is 27 kg/m^3 (0.87%wt) in Salado brine and 25 kg/m^3 in Castile brine for 100% enriched Pu—Fig. 13 and Table VI).

The critical concentration for 93% and 5% enriched UO_2 is 45 kg/m^3 and 1600 kg/m^3 (34%wt), respectively (Fig. 13).
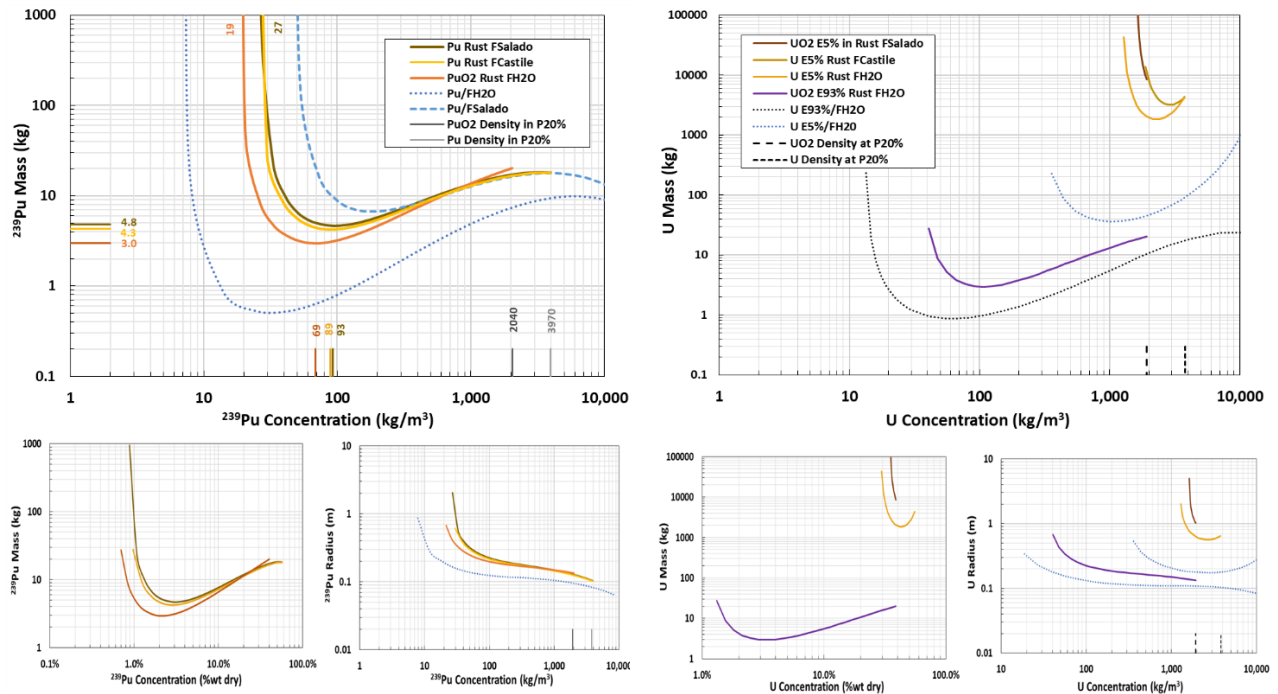
Fig. 13. Critical limits of fissile material with goethite at 20% porosity in water and WIPP brines (a) 100% enriched plutonium concentration, (b) 93% and 5% enriched uranium concentration, (c) plutonium concentration as %wt, (d) plutonium radius, (e) uranium concentration as %wt, (f) uranium radius.

IV.D. Fissile Critical Limits in SiO₂-Rich Materials

Silicon-rich materials such as volcanic tuff at Yucca Mountain[20, App. A] and sandstone were also considered for comparisons (Table III). Generally, SiO_2 acts as a weak moderator and reduces the critical concentration to less than for water (e.g., 9 kg/m^3 for 93% enriched ^{235}U in sandstone—from Fig. 14 or 12 kg/m^3 in water—Fig. 6). A strong solid moderator like graphite reduces the critical concentration even more (e.g., ~0.2 kg/m^3 for 93% enriched ^{235}U in graphite[31, Fig. 8])

IV.D.1. Sandstone

Uranium deposition, as UO_2, often occurred in permeable sandstone. Deposits in Wyoming and the Colorado Plateau, which represent ~30%wt of the world`s uranium reserves, are low-grade ores with between 0.1%wt and 3%wt UO_2. Similarly, a sandstone formation formed 2.15 ×10^9 years ago (2.15 Ga) in Gabon, Africa, also consists mostly of low grade (0.2-1 %wt uranium) (Table III).[19, Table 3; 37] However, some high concentrations of uraninite (UO_2) (>20 wt% uranium with porosity between 20% and 40%) were formed in the Oklo ore body. Some thin lenticular regions within the high concentration of uraninite operated as natural reactors 1.95 Ga, when natural uranium had a content of ~3.7 wt% ^{235}U (Fig. 14).[38]
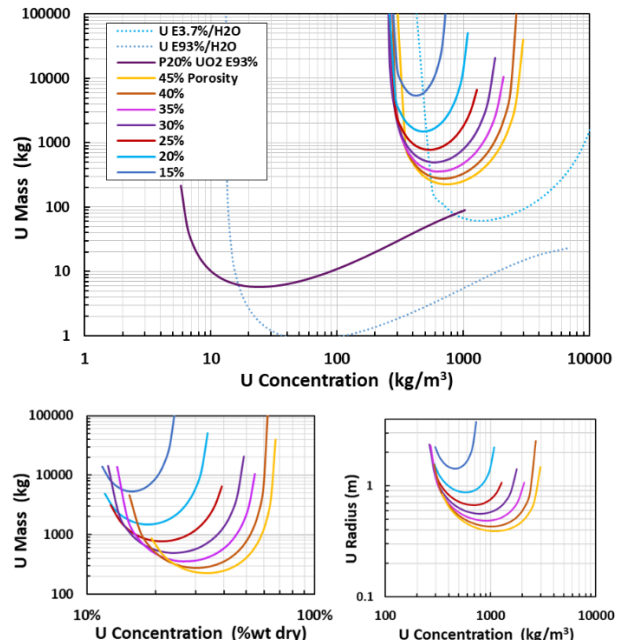
Fig. 14. Critical behavior for 3.7% enriched UO_2 in sandstone at porosities between 15% and 45%.

Deposition of a homogeneous sphere of 3.7% enriched uranium in Oklo sandstone (Table III) requires a high-grade ore (i.e., >210 kg/m^3 or 8.7 wt%) to go

critical.[b] The minimum critical mass varies between 554 kg at 20% porosity and 215 kg at 40% porosity.[38]

For PuO_2 at 100% enrichment in homogeneous sandstone, the minimum critical concentration is 3.3 kg/m^3 and the minimum critical mass is 2.85 kg at 20% total (and matrix) porosity (Fig. 15). In comparison, UO_2 at 93% enrichment, the minimum critical concentration is ~5 kg/m^3 and minimum critical mass is 5.7 kg (Fig. 14).
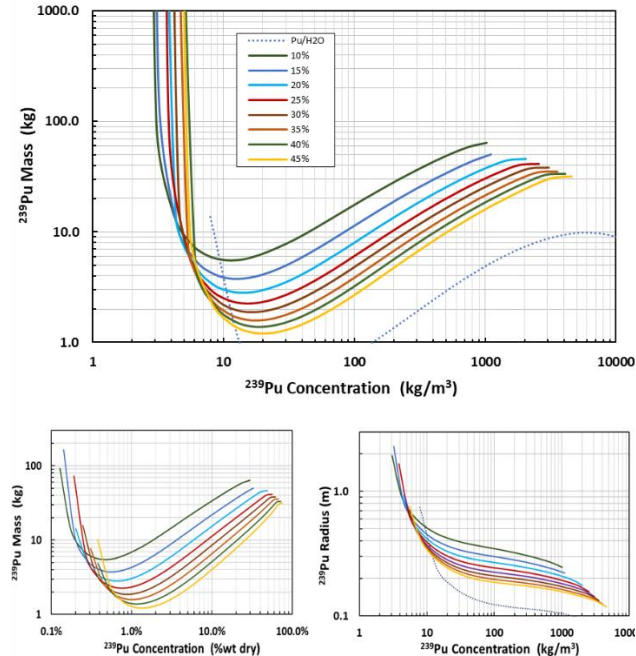
Fig. 15. Critical behavior for 100% enriched PuO_2 in sandstone at porosities between 10% and 45%.

IV.D.2. Tuff and Basalt

Volcanic tuff has only slightly less SiO_2 than sandstone (74% versus 84%—Table III) and so acts similar for 20% porosity saturated with water. The minimum critical concentration of 3.4 kg/m^3 is similar to 3.1 kg/m^3 for sandstone, and the minimum critical mass of 3.3 kg is similar to 3.7 kg—Fig. 16). Basalt has much less SiO_2 (48% versus 84%—Table III) and, thus, less moderating properties; the minimum critical concentration increases to 5 kg/m^3, and the minimum critical mass increases to 5.2 kg (Fig. 16).
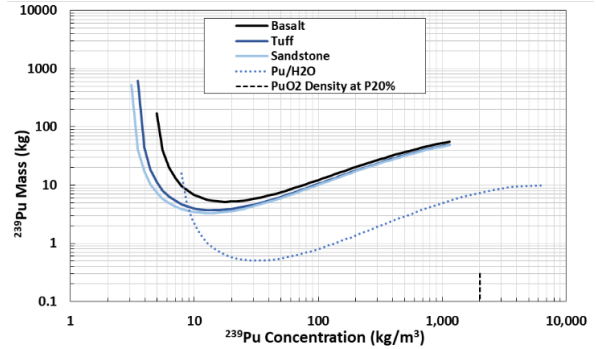
Fig. 16. Critical behavior similar for ^{239}Pu and water in sandstone, tuff, and basalt at 20% porosity.

IV.D.3. Fissile Critical Limits in Concrete

Concrete is present in the WIPP repository both as structural components and encapsulating waste. Cement in concrete does not have a fixed composition, but the major components are SiO_2, CaO, MgO, Al_2O_3, Na_2O, and Fe_2O_3. For concrete used in repository structures (e.g., drifts, shafts, and boreholes) where deposition of mobile Pu might occur, a cement composition high in SiO_2 content was used as specified by the Nuclear Regulatory Commission (NRC) (Table III).

The 6.6 MT non-pit Pu metal (§II.A.2) is likely to be oxidized to PuO_2 and encapsulated with a cement-like material and H_2O to form concrete but without any aggregate. [18] A simplified composition (termed CCO) was used that consisted of 65% SiO_2, 22% MgO, and 13% Al_2O_3 with a density of 2400 kg/m^3(or 58.5%, 19.8%, and 11.7% including 10% H_2O—Table III). The cement proportions were selected to be reasonably consistent with common cement compositions.[18] The NRC-concrete porosity is assumed to vary between 10% and 20%; the CCO-concrete, between 10% and 30%.

NRC-concrete, with high SiO_2 content, has a smaller minimum mass than CCO-concrete, with much higher Mg and Al content in both water and Salado brine. The critical concentrations of NRC and CCO concrete in water are similar, the concentrations vary between 3.0 and 4.1 kg/m^3 (Fig. 17). These critical concentrations are less than a Pu/H_2O mixture because of the moderated influence of SiO_2.

---

[b]Researchers usually analyze Oklo reactors using thin cylindrical shapes to better match the actual thin lenticular shape.[39] We use homogeneous spheres to be consistent with analysis reported here.
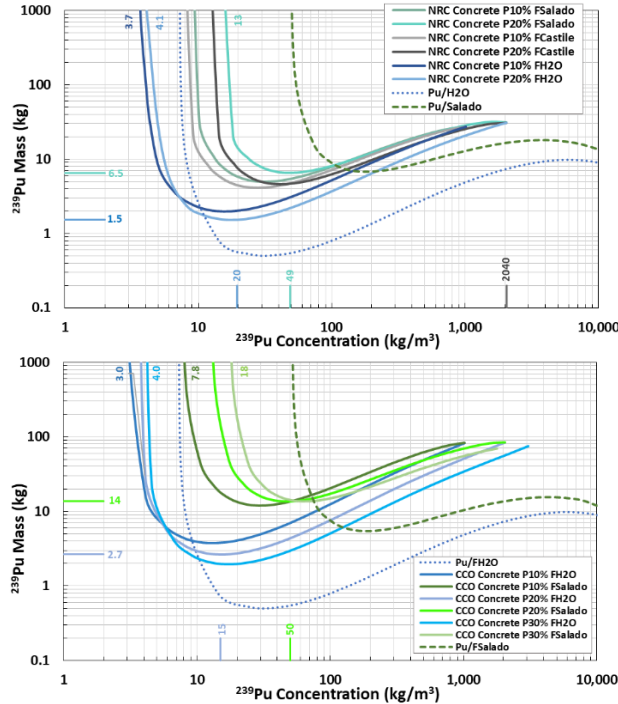
Fig. 17. Critical limits of 100% enriched Pu in various concrete mixtures with water and Salado WIPP brine (a) NRC concrete, and (b) simplified CCO concrete.

For NRC and CCO concrete in Salado brine, the critical concentration increases as the porosity increases. However, the minimum critical mass remains fairly constant as concrete porosity increases from 10% to 30%. At 30% porosity, the CCO-concrete critical mass is larger and must eventually decrease to the critical mass of a Pu/Salado mixture (i.e., 100% media porosity). In contrast, however, the NRC-concrete critical mass is already similar to the critical mass of a Pu/Salado mixture. The large amount of Cl^{-1} and B^{+3} evidently compensates for the additional hydrogen available in the pores.

IV.E. Fissile Critical Limits in Homogeneous Culebra Dolomite

For a homogeneous mixture of 100% enriched $^{239}PuO_2$ in Ca/Mg-rich Culebra dolomite saturated with Culebra brine at a common total available porosity in the Culebra of 20%, the minimum concentration and mass are 3.7 kg/m^3 and 2.3 kg, respectively (Fig. 18a and Table IV). A decrease in porosity in mildly moderating material shifts the curves to the left: for 15% total available porosity, the minimum concentration for criticality is 3.3 kg/m^3 and similar to the 3 kg/m^3 used in arguments screening out criticality for the CCA-1996.[1] The critical minimum mass is 2.4 kg.
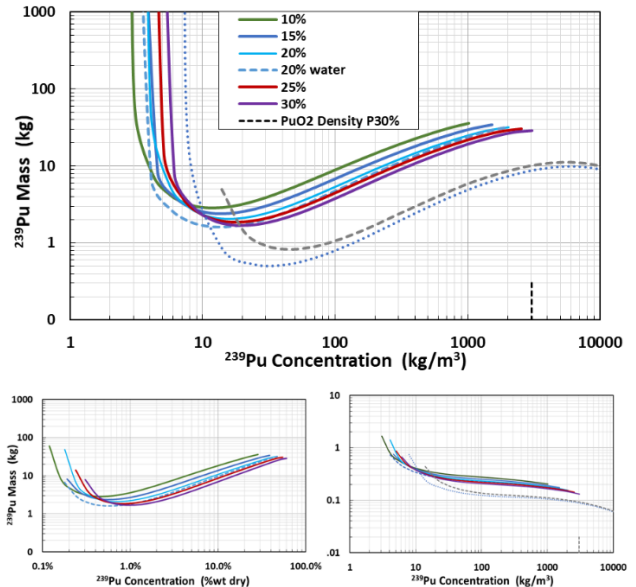
Fig. 18. Critical concentrations and masses for 100% enriched PuO_2 in homogeneous Culebra dolomite saturated with Culebra brine and total porosity between 10% and 30%.

To reach a critical concentration of 3.3 kg/m^3 in the Culebra, requires deposition conditions that would produce at least a low-grade ore (1300 ppm or 0.13 %wt dry at 15% porosity in 2816 kg/m^3 dolomite with PuO_2 filling pores—Fig. 18b).

Fig. 19. Criticality limits for UO_2 5% enriched ^{235}U in homogeneous mixture with various total porosities of Culebra dolomite saturated with Culebra brine.

For uranium as uraninite (UO_2) 5% enriched, the minimum concentration and mass are ~200 kg/m^3 (8.5 wt%) and 320 kg, respectively for a homogeneous model of the Culebra where all 23% total porosity is available

for deposition (i.e. 16% matrix, 5% vug, and 4% fracture porosity—Table IV). When expressed as ^{235}U, the minimum concentration and mass are 10 kg/m^3 and 16 kg, respectively (Fig. 19a). The maximum concentration when only the fracture porosity of 4% is available for fissile deposition is 390 kg/m^3 as uranium (19 kg/m^3 as ^{235}U).

At 15% enrichment in a homogeneous mixture, UO_2 (uraninite) and UO_2CO_3 (Rutherfordine) have the same critical concentration asymptote. They also have the same critical minimum mass (54 kg/m^3 and 40 kg, respectively) provided all the porosity is available for deposition (Fig. 20).

Fig. 20. Critical concentration of uranium as UO_2CO_3 and UO_2 at various enrichments in Culebra dolomite with 23% total porosity.

However, the minimum critical mass may differ if the porosity is restricted. If only 4% fracture porosity is available, the minimum masses of UO_2 and UO_2CO_3 differ slightly because of the larger volume of UO_2CO_3 (40 kg versus 42 kg, respectively). The minimum masses differ only slightly because the 4% fracture porosity can accommodate both the UO_2CO_3 and UO_2 at the minimum of ~41 kg at 15% uranium enrichment (Fig. 20).

The difference increases as the uranium enrichment decreases when porosity is restricted. At 5% enriched uranium, a homogeneous model of the Culebra with only 4% fracture porosity available is critical at ~300 kg when deposited as UO_2 but is critical only at masses above 10^4 kg when deposited as UO_2CO_3.

IV.F. Fissile Critical Limits in Limestone

The minimum critical concentration and mass for Ca-rich limestone with 20% total porosity is 3.0 kg/m3 and 2.84 kg in water (Fig. 21). The high Ca content (43%) in limestone acts as a weak moderator like Ca/Mg in Culebra dolomite and SiO$_2$ in sandstone and NRC-concrete.

Fig. 21. Behavior of Pu in limestone and Culebra dolomite influenced by calcium moderation and similar to silicon moderation in sandstone and NRC-concrete.

V. CRITICAL LIMITS CONSIDERING HETEROGENEITY IN CULEBRA DOLOMITE

V.A. Modeling Approach for Fracture Heterogeneity

As noted in §II.B.3, the Culebra dolomite has an advective porosity along bedding planes and fractures. Furthermore, the matrix porosity may be inaccessible except by diffusion and so fissile deposition may only occur in the fracture porosity. Hence, fissile deposition is more accurately modeled as heterogeneous in the Culebra dolomite. To evaluate the heterogeneity effects, we developed a model of fissile deposition in fractures of the Culebra. Besides the 5 parameters for the homogeneous model, the heterogeneous fracture model requires 3 additional parameters for the fracture porosity: (6) fracture/void porosity ($\bar{\phi}_{frac}^{void}$), (7) fraction of the void that is filled with fissile material (0< $f_{frac}^{fissile}$ <1.0), and (8) the fracture spacing (2B). In the calculation of the atom densities (Eq. (3)) the bulk densities are now

$$\rho_{bulk}^{fissile} = \rho^{fissile}[\phi^{matrix} f_{matrix}^{fissile}(1-\phi^{frac}) + \phi^{frac} f_{frac}^{fissile}] \quad (5)$$

$$\rho_{bulk}^{fluid} = \rho^{fluid}[\phi^{matrix}(1-f_{matrix}^{fissile})(1-\phi^{frac}) + \phi^{frac}(1-f_{frac}^{fissile})] \quad (6)$$

$$\rho_{bulk}^{rock} = \rho^{rock}(1-\phi^{matrix})(1-\phi^{frac}) \quad (7)$$

These expressions are derived from Eq. (4), by substituting in Eq. (2) and combining the vug and matrix porosity as an equivalent porosity ($\phi^{mat/vug}$) since fissile deposition in the vugs and matrix was not assumed); specifically,

$$\phi^{matrix} \text{of Eq. (3)} \rightarrow \phi^{total} = \phi^{frac} + \phi^{mat/vug}(1-\phi^{frac}) \quad (8)$$

$$f_{matrix}^{fissile} \text{of Eq.(3)} \rightarrow \begin{cases} f_{matrix}^{fissile} \text{for matrix} \\ f_{frac}^{fissile} \text{for fracture} \end{cases} \quad (9)$$

18 November 2019

The fracture porosity was usually set at a maximum of 4% ($0.1\% < \phi^{frac} < 4\%$); the matrix porosity of intact Culebra varied between 10 and 25% but was often set at a moderate value of 16% ($10\% < \phi^{matrix} < 25\%$). The fracture spacing (2B) was often set at 0.05 m but varied as low as 0.01 m to examine the sensitivity (0.05 m < 2B < 1 m range expected in Culebra).

Like the homogeneous model, the core sphere was surrounded by a spherical reflector of the same Culebra dolomite-brine mixture with a radius 2 m greater than the core (r^{core} +2 m) (Fig. 22). The criticality model for heterogeneous array of fractures was built with SCALE v6.2.1. To model the heterogeneity of the rock-liquid-fissile material system with a Monte Carlo code such as MCNP is difficult because of the large number of fractures needed to predict large critical masses (tens to hundreds of kilograms).

The spacing between fissile-containing fractures in the Culebra dolomite matrix defined the pitch between unit cells. The nuclear cross-sections for an array of repeating unit cells were processed by the BONAMI and CENTRUM modules of SCALE to adjust self-shielding and resonance absorption/flux depressions to include small-scale heterogeneity effects (i.e., include neutron interactions between nearby masses lumped in the fractures). This is a modern integral transport capability that faithfully models many of the characteristics of Wigner-Seitz cells required to generate volume averaged cross sections that heretofore have only been addressed in an approximate manner. Kastenberg et al. used a similar approach when evaluating critical potential from Pu deposition in volcanic tuff but used the older NITAWL module instead of CENTRUM.[40]

The calculations were then performed using the deterministic XSDRN module, like the fully homogeneous spherical model but using the nuclear cross-sections that included the heterogeneity effects of the repeating array of fracture unit cells.

V.B. Plutonium Critical Limits in Culebra Fracture Array

The minimum critical concentration is ~3.7 kg/m^3 in a heterogeneous fracture array in the Culebra spaced 5 cm with 18% total porosity (5% vug porosity, 4% fracture porosity, and 10% matrix porosity—Table IV) (Fig. 23). This minimum critical concentration does not differ substantially from the minimum critical concentration from a homogeneous model discussed previously in §IV.E. When these heterogeneous results are more meaningfully compared to a homogeneous model with 4% maximum available porosity (since deposition is confined to the fracture porosity) the minimum critical concentrations are very similar.
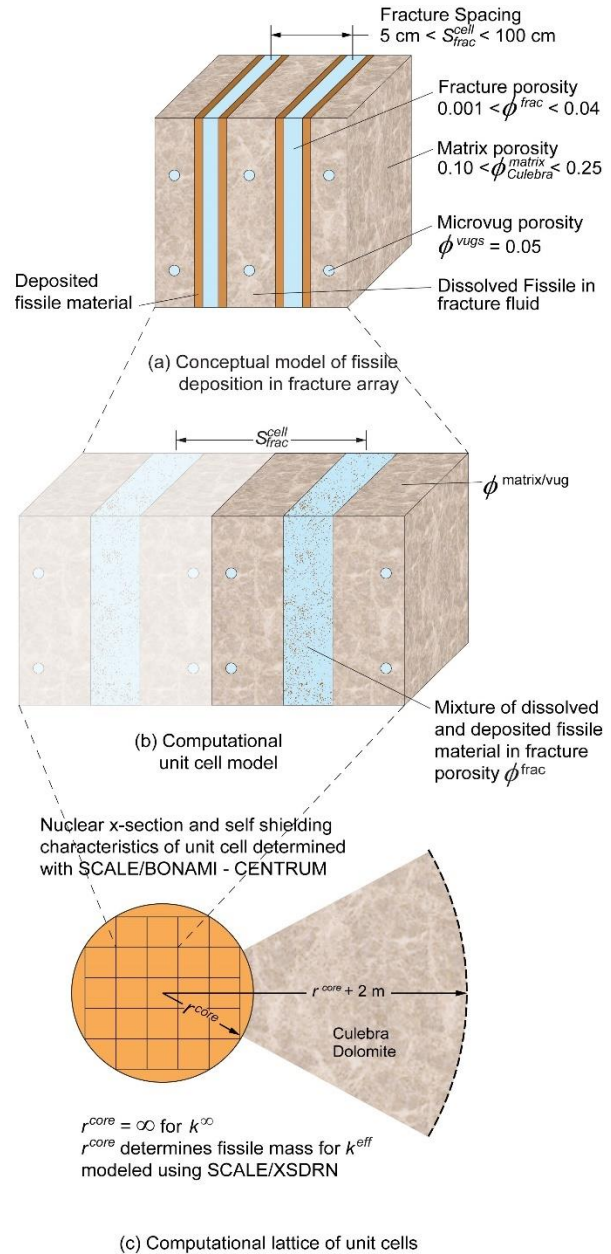
Fig. 22. Model for heterogeneous fracture deposition in Culebra dolomite of geologic barrier.

However, masses are noticeably different. Masses are less for Pu concentrations > 20 kg/m^3 (1 %wt) at 19% total porosity (Fig. 23) when the close spacing, high density of ^{239}Pu in a heterogenous configuration increases the interaction efficiency of high energy neutrons. Furthermore, the fracture heterogenous minimum mass is less than the homogeneous model with 4% of the porosity available for deposition when matrix porosities < 15%. However, heterogeneous masses are never less than the homogeneous model where the entire matrix porosity is available for deposition. That is, the maximum pore space for fissile material is 4% in the

homogeneous model in Fig. 23 while the maximum pore space for fissile material in Fig. 18 is 20%; hence, the critical masses are larger in Fig. 23.
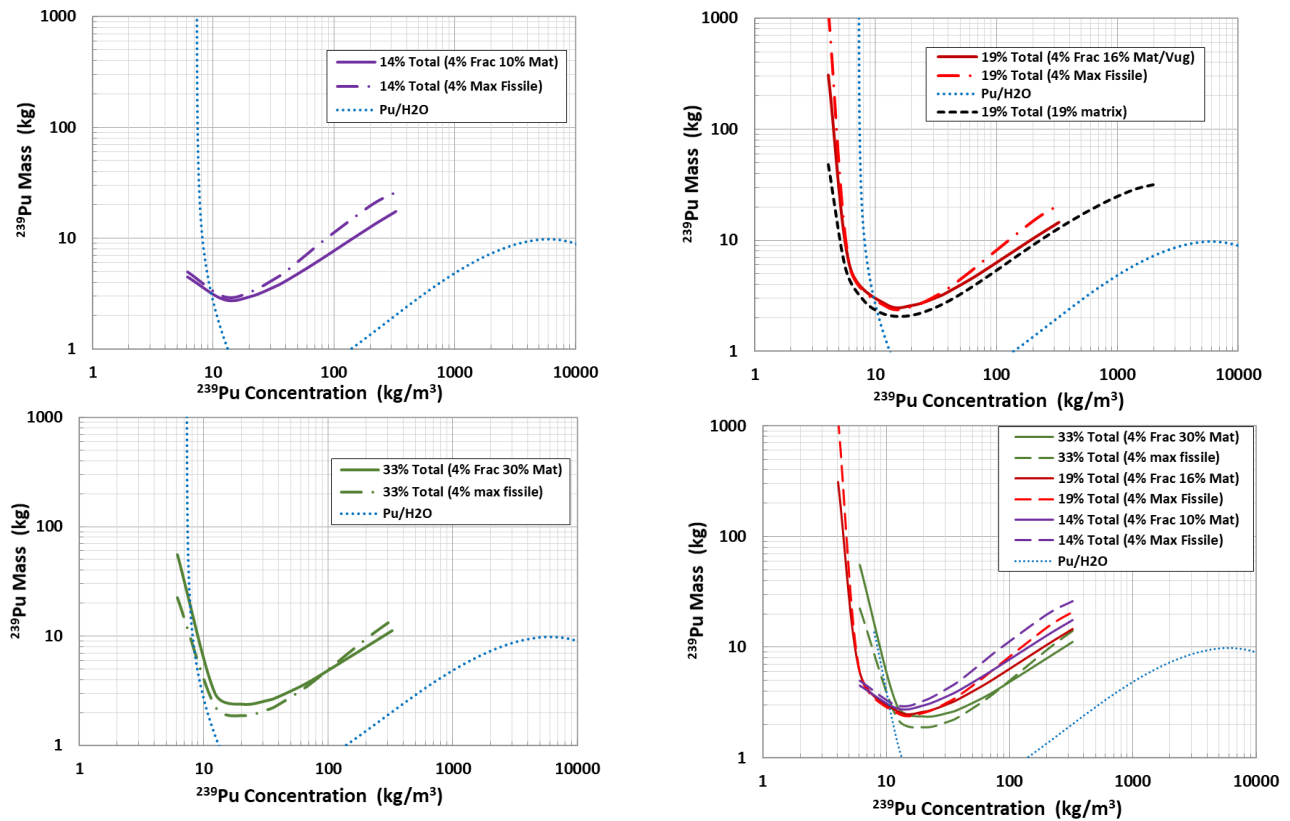
Fig. 23. Critical masses and concentrations of 100% enriched PuO_2 in the Culebra at variable matrix porosity as homogeneous mixture and as heterogenous planar fractures at 0.05 m spacing and 4% fracture porosity for deposition.
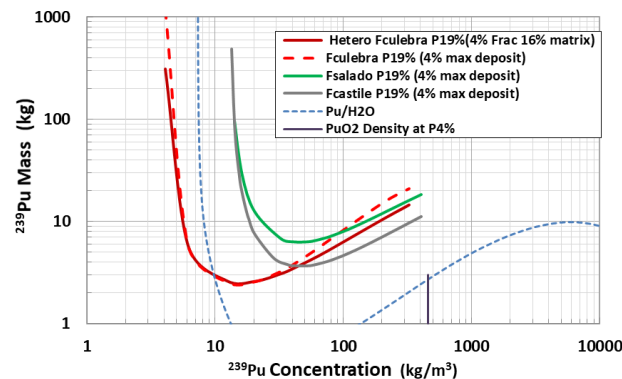
Fig. 24. Salado and Castile brines in 16% matrix porosity strongly influence critical mass and concentration for deposition of 100% enriched PuO_2 in 4% fracture porosity in Culebra dolomite.

As expected from the high concentrations of chloride (Table IV), the critical concentration noticeably increases for the Castile and Salado brines to 12 kg/m^3 at 19% total porosity (Fig. 24).

V.C. Uranium Critical Limits in Culebra Fracture Array

For 93% enriched uranium, the minimum critical ^{235}U mass is 4.6 kg, and the minimum asymptotic concentration is 6.6 kg/m^3 at 19% total porosity (16% matrix and 4% fracture) (Fig. 25). As previously noted, the U mineral is unimportant at high enrichment (Fig. 8).

For uraninite (UO_2) 5% enriched, the minimum concentration and mass are ~200 kg/m^3 (8.5 %wt) and 320 kg, respectively for a homogeneous Culebra model where all 23% total porosity is available for deposition, as presented earlier (Fig. 19). A heterogeneous Culebra model with 23% total porosity with 4% fracture porosity available for deposition is critical at similar masses. The fracture spacing is influential down to ~5 cm (Fig. 26).

18 November 2019
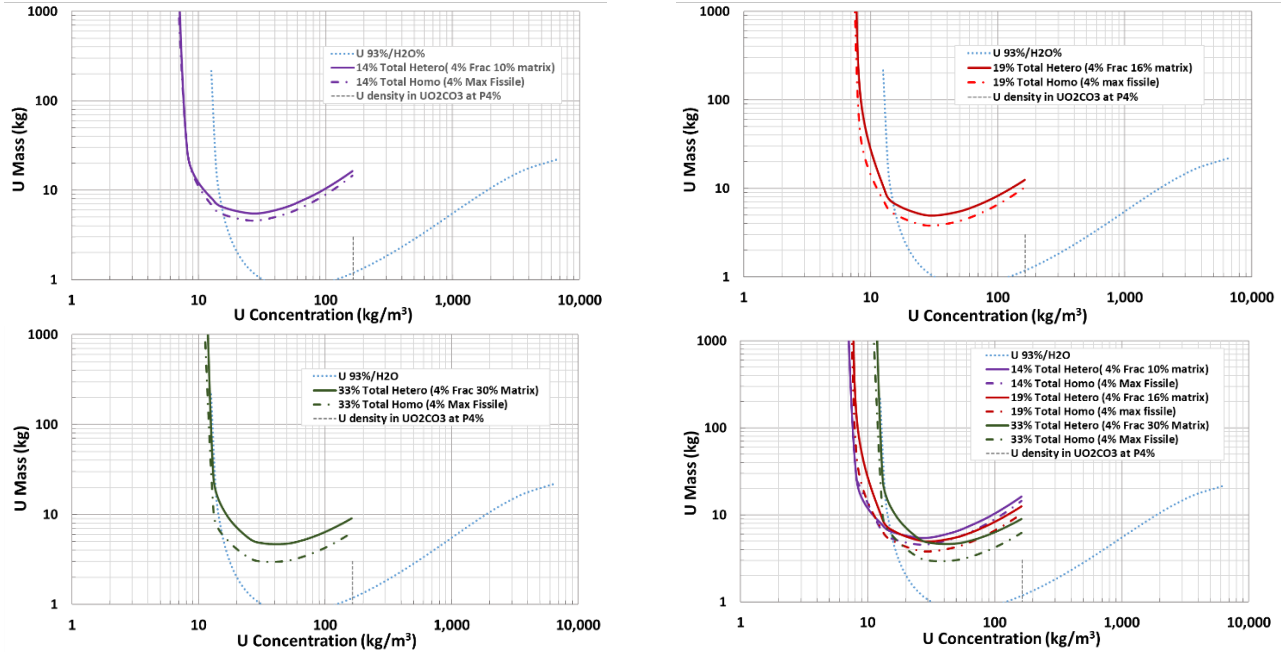
Fig. 25. Critical masses and concentrations of 93% enriched Rutherfordine in the Culebra at various matrix porosities as homogeneous mixture and as heterogenous planar fractures at 0.05 m spacing and 4% fracture porosity for deposition.
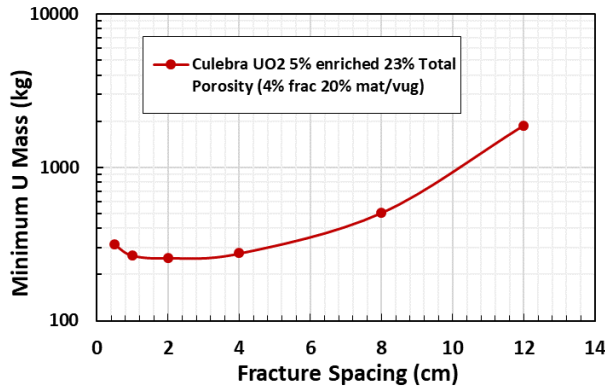
Fig. 26. Culebra fracture spacing < 5 cm has minor influence on minimum mass deposited as UO_2 at 5% enrichment with 23% total porosity (4% fracture porosity and 20% matrix/vug porosity)

VI. CONCLUSIONS

VI.A. Geologic Media Increases Critical Mass But Often Decreases Critical Concentration

In general, the addition of geologic media to a fissile/water binary system substantially increases the mass of fissile material necessary to go critical for ^{239}Pu (Fig. 27) and ^{235}U. In salt, the mass of 5% uranium required almost exceeds the amount of uranium to be placed in WIPP. The exception is hydrated montmorillonite clay with sufficient bound water present

such that the fissile material is optimally moderated even in the presence of clay components Si_4O_{10} and $Al_2(OH)_6$.

The influence of geologic media on the asymptotic limiting concentration varies (theoretically calculated by setting the divergence term in the Boltzman differential-integral neutron transport equation to zero and solving for $k^\infty=1$). For geologic material primarily composed of absorbing elements such as iron in rust or chloride in salt, the geologic material increases the critical concentration compared to fissile/water binary system (Fig. 27).
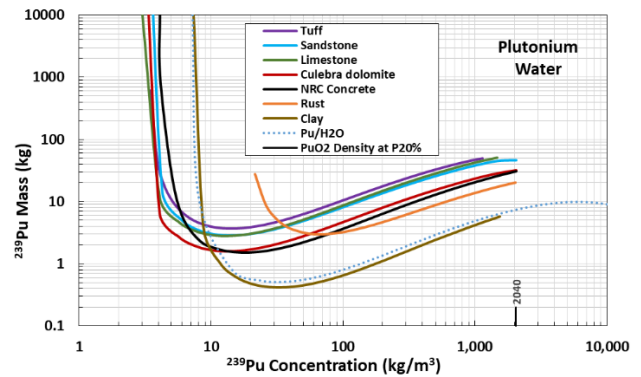
Fig. 27. Critical limits for PuO_2 100% enriched deposited in various material at 20% total porosity saturated with water

For geologic material primarily composed of weak moderators such as silicon, it decreases the critical concentration. Specifically, the minimum concentration

and mass in sandstone and volcanic tuff are similar because of the moderating influence of SiO_2 (74% and 84% when oxidized to SiO_2—Table III). Also, critical concentrations of limestone and Culebra dolomite are similar to sandstone because of the moderating influence Ca^{+2} and Mg^{+2} (91.5%). Finally, NRC-concrete, which is also composed of weak moderators (SiO_2 with some CaO and Al_2O_3) behaves similarly (particularly like Culebra dolomite).

VI.B. Brine Fluids Strongly Increase Critical Limits for Homogeneous Fissile Material

The substitution of WIPP brines for water in a fissile/fluid binary system substantially increases the fissile mass concentration necessary to go critical for ^{239}Pu (Fig. 28) and ^{235}U (Table VI).
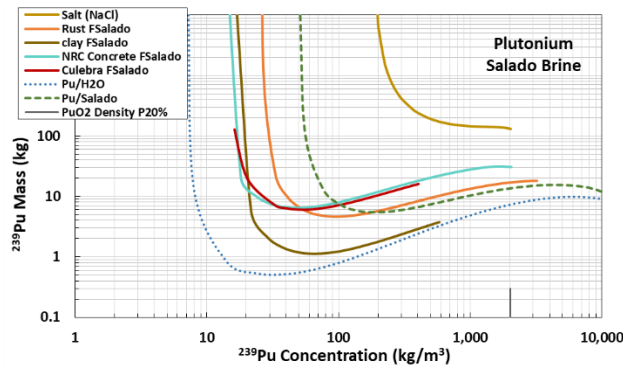
Fig. 28. WIPP Salado brine substantially increases critical limits for PuO_2 100% enriched deposited in various materials at 20% total porosity.

VI.C. Porosity has Strong Influence on Critical Mass and Concentration.

The porosity of the geologic media has a strong influence on both the critical mass and the critical concentration in brine and water. As the porosity increases, the behavior approaches that of a fissile/fluid binary system, and the critical mass decreases (Fig. 29).
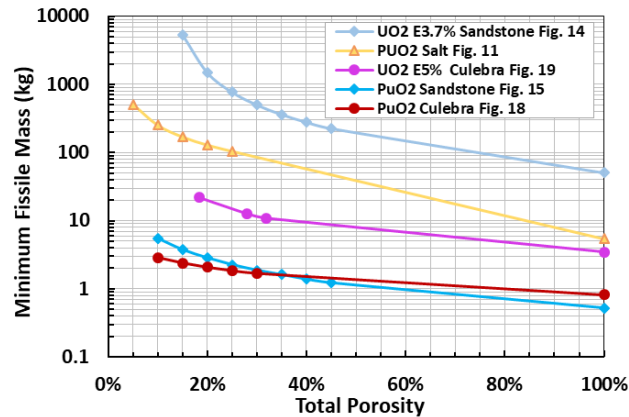
Fig. 29. Minimum fissile mass decreases with increase in geologic porosity as geologic media influence on reactivity decreases.

The influence of porosity increase on the asymptotic critical concentration depends on whether the geologic material is primarily a weak moderator such as Culebra dolomite, which increases asymptotic concentration, or a neutron absorber such as salt or rust, which decreases asymptotic critical concentration (Fig. 30).
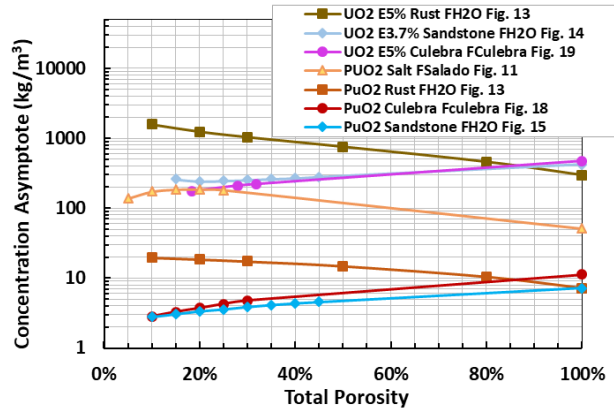
Fig. 30. Minimum critical concentration asymptote increases with porosity increase for weak moderators, such as Culebra dolomite, and decreases with porosity increase for neutron absorbing material, such as salt and rust.

VI.D. Fracture Heterogeneity of Culebra Dolomite has Minor Influence on Critical Concentration

The Culebra dolomite is most accurately modeled as fractured heterogenous media with deposition primarily limited to the fractures. Media heterogeneity is influential on the minimum critical mass (Fig. 31) but less so on the minimum critical concentration (Fig. 32).

A homogeneous model with deposition in only 4% of the porosity is bounding except when the minimum critical concentration of a heterogeneous model with 4% fracture porosity is slightly less when porosity < 18%, (Fig. 31). Hence, heterogeneity is important when deposition only occurs is portion of the porosity (here the fracture porosity) and the total porosity is small, even at high enrichment. Nonetheless, a homogeneous model with ^{239}Pu deposition in all the porosity bounds both the minimum critical concentration and mass of a heterogeneous model.

To elaborate, the minimum critical concentration of 4 kg/m^3 at 18% total porosity (minimum porosity in Table IV for 4% fracture porosity) for a heterogeneous model is the same as a homogeneous model with maximum deposition in 4% of the porosity but is bound by the 3.7 kg/m^3 minimum critical concentration for a fully homogeneous model (and the 3 kg/m^3 for the homogeneous model used previously in the 1996 CCA).

18 November 2019
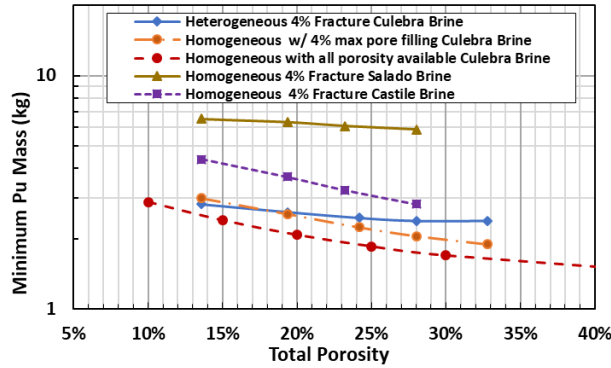
Fig. 31. Critical Pu mass for homogeneous models less than for heterogeneous model when total porosity >18% with 4% fracture porosity in Culebra.
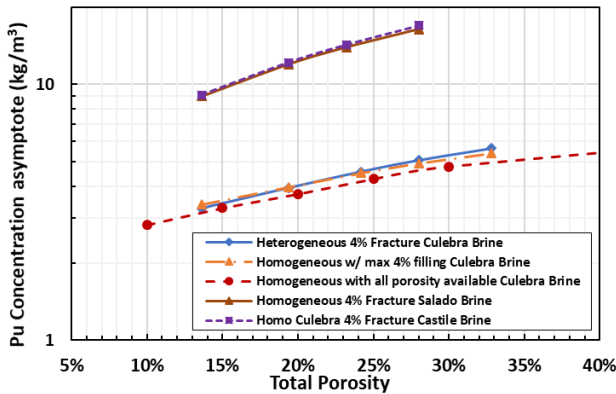
Fig. 32. Minimum critical concentration for a mixture of infinite mass and extent influenced by total porosity and pore fluid type but not media heterogeneity in Culebra dolomite.

However, the situation near the minimum critical mass does not tell the whole story since when ^{239}Pu is under moderated (high ^{239}Pu concentration), the heterogeneous model is bounding (less mass). At high ^{239}Pu concentration, high energy neutrons released in fission can migrate through the geologic media/fluid system and miss the large resonances in the non-fissile isotopes (Fig. 23).

As expected from the high concentrations of chloride (Table IV and Fig. 5), the critical mass and concentration noticeably increases for the Castile and Salado brines; specifically, 2.6 kg and 12 kg/m^3 at 19% total porosity for Salado brine (Fig. 31 and Fig. 32).[c]

VI.E. Summary

The neutronic criteria necessary for criticality in geologic media associated with WIPP, specifically, the minimum critical mass and concentration, suggest that deposition of large masses and concentrations are required for fissile material low in ^{235}U enrichment.

Homogeneous geologic systems are often more reactive at high enrichments. However, unlike engineered systems, heterogeneous geologic systems are not always more reactive at low enrichments because the relationship between the porosity of the fractures and matrix also strongly influences the results.

The mass of fissile material collected in a region of geologic material is dependent on elapsed time of deposition, unless geometrical constraints exist on the space available. In contrast, the asymptotic criticality concentration limits calculated here for an infinite media system are most often used in companion papers to demonstrate the lack of criticality concern for three reasons: Concentration limits are (1) more readily compared to geologic processes such as precipitation, adsorption, and colloidal aggregation/filtration, (2) mostly independent of elapsed time, and (3) less influenced by the heterogeneity of the media (Fig. 32).

ACKNOWLEDGEMENTS

REFERENCES

1. R. P. RECHARD, L. C. SANCHEZ, H. R. TRELLUE and C. T. STOCKMAN, "Unfavorable Conditions for Nuclear Criticality Following Disposal of Transuranic Waste at the Waste Isolation Pilot Plant," *Nuclear Technology*, **136**(*1*), 99-129 (2001).

2. R. P. RECHARD, L. C. SANCHEZ, C. T. STOCKMAN and H. R. TRELLUE, "Consideration of Nuclear Criticality When Disposing of Transuranic Waste at the Waste Isolation Pilot Plant," SAND99-2898, Sandia National Laboratories (2000).

3. R. P. RECHARD, "Probability and Consequences of Nuclear Criticality at a Geologic Repository--I: Conceptual Overview for Screening," *Nuclear Technology*, **190**(*2*), 97-126 (2015).

---

[c] Results and figures have been archived in the WIPP Centrat Files under /nfs/data/CVSLIB/WIPP_EXTERNAL/CRA19_crit/FILES.

18 November 2019

4. DOE (US DEPARTMENT OF ENERGY), "Surplus Plutonium Disposition, Record of Decision," *Federal Register*, **81**(*65*), 19588-19594 (2016).

5. R. P. RECHARD and E. STEIN, "Hydrologic and Geochemical Constraints on Criticality in Geologic Media near Bedded Salt Repository; Memorandum to Paul E. Shoemaker, 8880; Todd Zeitler, 8863; Ross Kirkes, 8883; November 2019," Sandia National Laboratories (2019).

6. R. P. RECHARD, "Improbability of Transuranic Waste Compaction by Salt Creep Causing Criticality in Bedded Salt Repository; Memorandum to Paul E. Shoemaker, 8880; Todd Zeitler, 8863; Ross Kirkes, 8883; November 2019," Sandia National Laboratories (2019).

7. DOE (US DEPARTMENT OF ENERGY), "Title 40 CFR Part 191: Compliance Certification Application for the Waste Isolation Pilot Plant," DOE/CAO-1996-2184. Vol. I-XXI, DOE Carlsbad Area Office (1996).

8. C. D. LEIGH, J. TRONE and B. FOX, "Tru Waste Inventory for the 2004 Compliance Recertification Application Performance Assessment Baseline Calculation," ERMS 541118, Sandia National Laboratories (2005).

9. B. CRAWFORD, D. GUERIN, S. LOTT, W. MCINROY, J. MCTAGGART and G. D. VAN SOEST, "Performance Assessment Inventory Report--2008," INV-PA-08, Revision 0, Los Alamos National Laboratory, Carlsbad Operations (2009).

10. G. D. VAN SOEST, "Performance Assessment Inventory Report - 2012," INV-PA-12, Rev. 0; LA-UR-12-26643, Los Alamos National Laboratory Carlsbad Operations (2012).

11. G. D. VAN SOEST, "Performance Assessment Inventory Report--2018," INV-PA-18, Revision 0, Los Alamos National Laboratory (2018).

12. C. L. STEIN, "Mineralogy in the Waste Isolation Pilot Plant (WIPP) Facility Stratigraphic Horizon," SAND85-0321, Sandia National Laboratories (1985).

13. R. P. RECHARD, "Historical Background on Performance Assessment for the Waste Isolation Pilot Plant," *Reliability Engineering and System Safety*, **69**(*1-3*), 5-46 (2000).

14. M. G. MARIETTA, D. R. ANDERSON, G. BASABILVAZO, J. C. HELTON and H.-N. JOW, "Summary Discussion of the 1996 Performance Assessment for the Waste Isolation Pilot Plant," *Reliability Engineering and System Safety*, **69**(*1-3*), 437-452 (2000).

15. M. D. SIEGEL, S. J. LAMBERT and K. L. ROBINSON, "Hydrogeolchemical Studies of the Rustler Formation and Related Rocks in the Waste Isolation Pilot Plant Area, Southeastern New Mexico," SAND88-0196, Sandia National Laboratories (1991).

16. T. SEWARDS, A. BREARLEY, R. GLEN, I. D. R. MACKINNON and M. D. SIEGEL, "Nature and Genesis of Clay Minerals of the Rustler Formation in the Vicinity of the Waste Isolation Pilot Plant in Southeastern New Mexico," SAND90-2569, Sandia National Laboratories (1992).

17. L. BRUSH, H, "Test Plan for Laboratory and Modeling Studies of Repository and Radionuclide Chemistry for the Waste Isolation Pilot Plant," SAND90-0266, Sandia National Laboratories (1990).

18. E. M. SAYLOR and J. M. SCAGLIONE, "Nuclear Criticality Safety Assessment of Potential Plutonium Disposition at the Waste Isolation Pilot Plant," ORNL/TM-2017/751/R1, Oak Ridge National Laboratory (2018).

19. F. GAUTHIER-LAFAYE, F. WEBER and H. OHMOTO, "Natural Fission Reactors of Oklo," *Economic Geology*, **84**(*8*), 2286 (1989).

20. D. E. BROXTON, R. G. WARREN, R. C. HAGAN and G. LUEDERMANN, "Chemistry of Diagenetically Altered Tuffs at a Potential Nuclear Waste Repository, Yucca Mountain, Nye County, Nevada," LA-10802-MS, Los Alamos National Laboratory (1986).

21. P. C. GOODELL, "Geology of the Peña Blanca Uranium Deposits, Chihuahua, Mexico. Uranium in Volcanic and Volcaniclastic Rocks," *AAPG Studies in Geology. American Association of Petroleum Geologists*(*No. 13*), 275 (1981).

22. L. C. MEIGS, R. L. BEAUHEIM, J. T. MCCORD, Y. W. TSANG and R. HAGGERTY, "Design, Modelling, and Current Interpretations of the H-19 and H-11 Tracer Tests at the WIPP Site," *Field Transport Experiments: Role in the Prediction of Radionuclide Migration: Synthesis and Proceeding*

of an NEA/EC GEOTRAP Workshop, Cologne, Germany, August 28-30, 1996, 157-169, Nuclear Energy Agency, Organisation for Economic Co-Operation and Development (1996).

23. R. P. RECHARD, "Historical Background on Assessing the Performance of the Waste Isolation Pilot Plant," SAND98-2708, Sandia National Laboratories (1999).

24. R. P. RECHARD and M. S. TIERNEY, "Assignment of Probability Distributions for Parameters in the 1996 Performance Assessment for the Waste Isolation Pilot Plant, Part 2: Application of Process," Reliability Engineering and System Safety, 88(1), 33-80 (2005).

25. R. P. RECHARD, A. C. PETERSON, J. D. SCHREIBER, H. J. IUZZOLINO, M. S. TIERNEY and J. S. SANDHA, "Preliminary Comparison with 40 CFR Part 191, Subpart B for the Waste Isolation Pilot Plant, December 1991, Volume 3: Reference Data," SAND91-0893/3, Sandia National Laboratories (1991).

26. H. W. PAPENGUTH and Y. K. BEHL, "Test Plan: Evaluation of Dissolved Actinide Retardation at the Waste Isolation Pilot Plant," TP 96-02. WPO 31336, Sandia National Laboratories (1996).

27. D. E. DEAL, R. J. ABITZ, D. S. BELSKI, J. B. CASE, M. E. CRAWLEY, C. A. GIVENS, P. P. J. LIPPONNER, D. J. MILLIGAN, J. MYERS, D. W. POWERS and M. A. VALDIVIA, "Brine Sampling and Evaluation Program, 1992-1993 Report and Summary of Bsep Data since 1982," (1995).

28. C.J. WERNER, et al., eds., MCNP® User's Manual, Code Version 6.2, LA-UR-17-29981, Los Alamos National Laboratory (2017).

29. J. J. DUDERSTADT and L. J. HAMILTON, Nuclear Ractor Analysis, John Wiley & Sons, (1976).

30. E. D. CLAYTON and W. A. REARDON, "Chapter 27: Nuclear Safety and Criticality of Plutonium." In Plutonium Handbook: A Guide to the Technology American Nuclear Society (1980).

31. H. C. PAXTON, J. T. THOMAS, D. CALLIHAN and E. B. JOHNSON, "Critical Dimensions of Systems Containing ^{235}u, ^{239}pu and ^{233}u," TID-7028, Los Alamos National Laboratory; Oak Ridge National Laboratory (1964).

32. R. P. RECHARD, L. C. SANCHEZ and H. R. TRELLUE, "Consideration of Nuclear Criticality When Directly Disposing Highly Enriched Spent Nuclear Fuel in Unsaturated Tuff, Part 1: Nuclear Criticality Constraints," Nuclear Technology, 144, 201 (2003).

33. T. W. LAMBE and R. V. WHITMAN, Soil Mechanics, John Wiley & Sons, (1969).

34. W. A. DEER, R. A. HOWIE and J. ZUSSMAN, An Introduction to the Rock-Forming Minerals, Longman, (1985).

35. C. LIU, Z. ZHU, F. LI, T. LIU, C. LIAO, J.-J. LEE, K. SHIH, L. TAO and Y. WU, "Fe(II)-Induced Phase Transormation of Ferrihydrite: The Inhibition Effects and Stabilization of Divalent Metal Cations," Geochemical Geology, 444, 110-119 (2016).

36. C. HANSEL, M., S. G. BENNER and S. FENDORF, "Competing Fe(II)-Induced Mineralization Pathways of Ferrihydrite," Envionmental Science Technology, 39(18), 7147-7153 (2005).

37. F. GAUTHIER-LAFAYE and F. WEBER, "Natural Nuclear Fission Reactors: Time Constraints for Occurrence, and Their Relation to Uranium and Manganese Deposits and to the Evolution of the Atmosphere," Precambrian Research, 120, 81-100 (2003).

38. F. GAUTHIER-LAFAYE, P. HOLLIGER and P. BLANC, "Natural Fission Reactors in the Franceville Basin, Gabon: A Review of the Conditions and Results of a "Critical Event" in a Geologic System," Geochimica et Cosmochimica Acta, 60(23), 4831-4852 (1996).

39. S.-E. BENTRIDI, B. GALL, F. GAUTHIER-LAFAYE, A. SEGHOUR and D.-E. MEDJADI, "Inception and Evolution of Oklo Natural Nuclear Reactors," Comptes Rendus Geoscience, 343, 738-748 (2011).

40. W. E. KASTENBERG, P. F. PETERSON, J. AHN, J. BURCH, G. CASHER, P. CHAMBRÉ, E. GREENSPAN, D. R. OLANDER, J. VUJIC, B. BESSINGER, N. G. W. COOK, F. M. DOYLE and B. HILBERT, "Considerations of Autocatalytic Criticality of Fissile Materials in Geologic Repositories," Nuclear Technology 115, 298-309 (1996).

APPENDIX A: VERIFICATION OF SCALE CRITICALITY LIMITS WITH MCNP

SUMMARY

A renewed evaluation of the feature, event, and process (FEP) on the likelihood of assembling a critical mass after closure in or near the Waste Isolation Pilot Plant (WIPP) has been undertaken for the Compliance Recertification Application for 2019 (CRA-2019). As part of this reevaluation, previously published calculations for ideal homogeneous spherical configurations of fissile material (either ^{239}Pu or ^{235}U) in the repository and geologic barrier conducted for the 1996 Compliance Certification Appliction (CCA-199) were verified with SCALE 6.1. In addition, critical limits (i.e., minimum critical asymptotic concentration, minimum critical mass and corresponding concentration and radius were verified with MCNP^{TM} 6.2 and are reported here (Figure ES-1). The criticality results are for homogeneous, spherical mixtures of fissile plutonium (^{239}Pu) and uranium (^{235}U) with salt (NaCl), rust— goethite ((FeO(OH)), NRC concrete, Culebra dolomite, pure water, WIPP Salado brine, WIPP Castile brine, and WIPP Culebra brine. When solid material was included in the homogeneous mixture, the solid porosity was set at 20%.
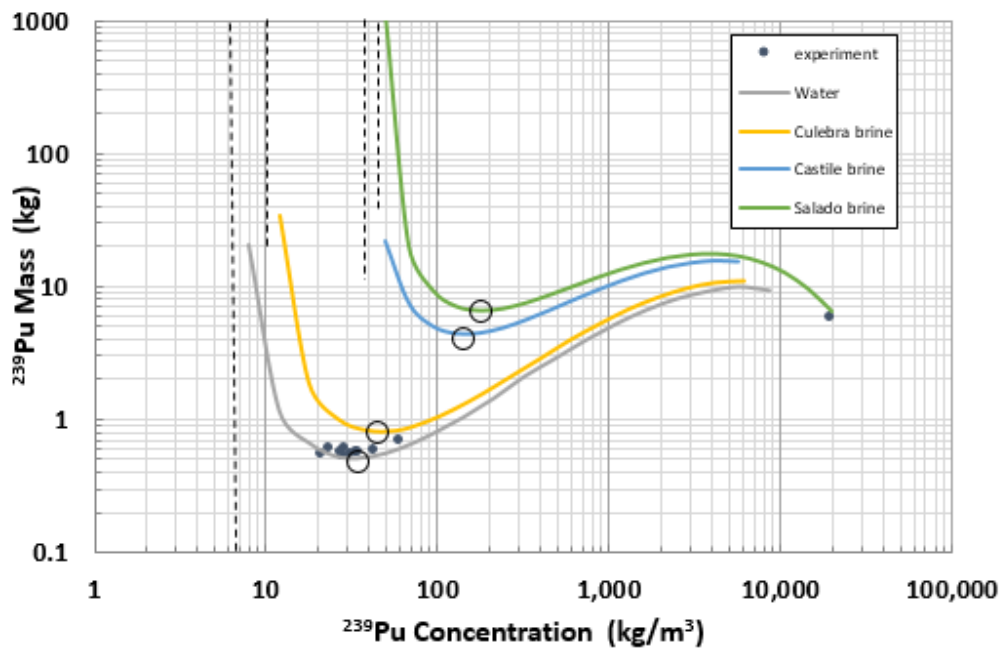
Figure A-1. The black circles on the criticality curve were k^{eff} is unity illustrates the minimum mass and corresponding concentration that are compared. The black dashed lines illustrate the minimum asymptotic concentration values that are compared.

18 November 2019

INTRODUCTION

This memo presents the minimum fissile mass (either ^{239}Pu or ^{235}U) needed to obtain criticality, with its respective concentration and radius in material associated with WIPP. The minimum asymptotic critical concentration is also estimated. The general purpose is to use MCNP (Monte Carlo code for solving Neutron and Photon transport equations) to verify results obtained with SCALE 6.1. Although the results are presented in the main body, this appendix also reports the atom densities of the homogeneous mixtures with and without fissile material, which are the key input for MCNP.

CALCULATION

Software
Two copies of the MCNP software, version 6.2, were acquired from RSICC[d] April 2019 and installed, using the supplied installation executable, on two personal laptops: Sus Vivobook F510UA and Asus Strix 17 GL703GE

Data
The Evaluated Nuclear Data File/B Version 7.1 (ENDF/B-VII.1) nuclear cross-sections were used, which are distributed along with MCNP version 6.2 (file xsdir_mcnp6.2_endfb-7.1). ENDF/B-VII.1 is maintained at the National Nuclear Data Center (NNDC) at Brookhaven National Laboratory (BNL) and are endorsed by the Cross Section Evaluation Working Group (CSEWG). In addition, the MCNP calculations used data from the Seventeenth Edition of the Chart of Nuclides.

The geologic data used in the analysis are reported in the main body; specifically, Table II, Table III, and Table V.

Results Retention
The MCNP input and output files are stored in the WIPP Central files for the CRA-2019 under the directory /nfs/data/CVSLIB/WIPP_EXTERNAL/CRA19_crit/FILES

Method

Spherical model
   In the MCNP model, a spherical core of fissile material and fluid in the pores of the geologic material is surrounded by a spherical reflector with a radius 2 m greater than the core to approximate a reflector of infinite extent (r^{core}+2m). The spherical reflector has the same composition as the spherical core, but the fissile component in the porosity is replaced with additional fluid (either water or brine).

Atom fractions of materials
The first step is calculating atom fractions of each material. For example for the Salado brine, we are given the moles of each molecule per meter cubed, the specific density, and the density of each material. Using this, we obtain the density of water in the material. An atom density calculation is then performed to help find the atom fractions and total atom density.

Atom density of outer sphere
For the outer sphere, we assume the brine takes up the entire porosity. The density of all the calculations use a porosity of 20%. Therefore, to calculate the atom density of the solid material, you must first multiply its density by 0.80. The solid material atom density remains constant through both the inner and outer sphere. For the brine, we multiply its density by the porosity.

Atom density of inner sphere
In the inner sphere the fissile fraction changes with the change in the concentration of plutonium. The calculation for the inner sphere is like the outer, except that there are two fractions used in this calculation: porosity and fissile fraction. The fissile fraction is the fraction of plutonium; the brine fraction is unity minus the fissile fraction. The

---

[d] RSICC (Radiation Safety Information Computational Center) is a Specialized Information Analysis Center (SIAC) of the US Department of Energy, which resides in the Reactor and Nuclear Systems Divisions (RNSD) at Oak Ridge National Laboratory that maintains computer software and data sets for radiation transport and safety analysis (see https://rsicc.ornl.gov/RSICCNewsLetters.aspx)

fissile material and brine takes up space in the pores of the solid material. Therefore, the change in concentration of the fissile material changes the fissile fraction in the pores. To calculate the fissile fraction, its concentration is divided by both the density of plutonium and the porosity, so that a volume fraction is obtained.

After we obtain the volume fraction of plutonium, we subtract it from unity to get the volume fraction of the brine. The fractions are then used in the atom density calculations to find the final atom densities and atom fractions for the inner sphere.

Search for minimum mass
The search for the minimum mass and concentration with MCNP starts with the rough SCALE estimation. Using an excel spreadsheet to automatically calculate the atom densities and fractions, points on the criticality S-curve are found. The concentration is held constant and the mass changed until the k^{eff} is unity. Then the mass is held constant and the concentration changed until k^{eff} is unity at a different concentration. The process is then repeated three times. MCNP was being ran using only 2000 active cycles.
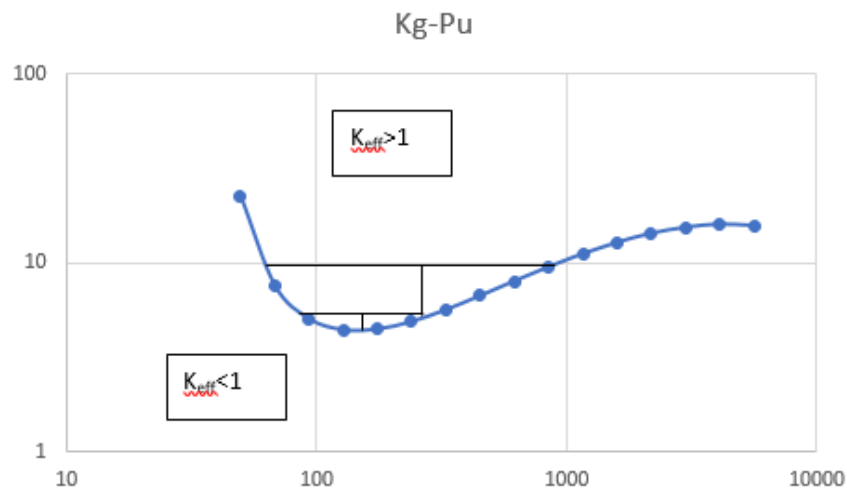
Figure A-2. Process of finding the minimum mass for criticality from initial guess

RESULTS
The results are presented in a series of four tables for 7 materials or fluids (where the appendix section corresponds to the 7 materials or fluids. For example, Section 1 is for Pu in WIPP brines, Section 2 is for Pu in goethite and WIPP brines that was used in the calculations.

Table	Description
Table A#-1	Contains comparative data between SCALE and MCNP for the minimum mass in each WIPP brine.
Table A#-2	Contains comparative data between SCALE and MCNP for the minimum concentration needed for criticality.
Table A#-3	Contains the calculated atom densities of elements in the WIPP brine mixtures without plutonium or uranium; the table also lists their Z charge and atomic number ID (ZAID).
Table A#-4	Contains the atom densities of elements in the different brine mixtures with plutonium or uranium included; the table also lists their ZAID.

Table A1-1. MCNP™computed k^{eff} values compared to SCALE criticality S-curves for minimum Pu mass in water and WIPP brines

Brine	SCALE			MCNP					
	Mass Min (kg)	Radius Min (m)	Conc at Min Mass (kg/m³)	Mass Min (kg)	Radius Min (m)	Conc at Min Mass (kg/m³)	k_{eff}	+/- error	M:F Ratio
Water	0.521133	0.14310	42.4562	0.504828	0.15571	31.9231	1.00013	0.00028	829.9990
Culebra	0.789335	0.15050	55.2794	0.799205	0.15220	54.1160	0.99997	0.0003	487.5207
Castile	3.690999	0.17720	158.3668	3.833199	0.17945	158.3668	1.00001	0.0003	151.4995
Salado	5.469572	0.18960	191.5798	5.325006	0.18880	188.8972	0.99999	0.00029	124.1716

Table A1-2. MCNP computed asymptote values compared to SCALE criticality S-curves for Pu mixed with water and WIPP brines

Brine	SCALE	MCNP
	Minimum kg/m³	Minimum kg/m³
Water	7.2272	7.2330
Culebra	11.2049	11.1695
Castile	40.9770	40.3999
Salado	51.2290	51.7200

18 November 2019

Table A1‑3. Atom densities of elements making up water and brine.

Isotopes	ZAID	Water atom/b*cm	Culebra atom/b*cm	Castile atom/b*cm	Salado atom/b*cm
H-1	1001	6.6847E-02	6.6635E-02	6.0858E-02	5.9719E-02
H-2	1002	7.6883E-06	7.6639E-06	6.9994E-06	6.8684E-06
O-16	8016	3.3427E-02	3.3508E-02	3.0866E-02	3.0593E-02
Na-23	11023		3.6132E-04	2.9327E-03	2.4750E-03
Mg-24	12024		9.9892E-06	9.0379E-06	2.9968E-04
Mg-25	12025		1.2646E-06	1.1442E-06	3.7939E-05
Mg-26	12026		1.3923E-06	1.2597E-06	4.1770E-05
K-39	19039		4.6613E-06	5.4475E-05	1.9656E-04
K-40	19040		5.8480E-10	6.8344E-09	2.4660E-08
K-41	19041		3.3639E-07	3.9313E-06	1.4185E-05
Ca-40	20040		1.3427E-05	7.0053E-06	4.4834E-06
Ca-42	20042		8.9613E-08	4.6755E-08	2.9923E-08
Ca-43	20043		1.8698E-08	9.7556E-09	6.2436E-09
Ca-44	20044		2.8892E-07	1.5074E-07	9.6475E-08
Ca-46	20046		5.5402E-10	2.8906E-10	1.8500E-10
Ca-48	20048		2.5901E-08	1.3513E-08	8.6486E-09
B-10	5010		3.3555E-07	7.5498E-06	1.7257E-05
B-11	5011		1.3506E-06	3.0389E-05	6.9460E-05
Cl-35	17035		2.5868E-04	2.1899E-03	2.3268E-03
Cl-37	17037		8.2767E-05	7.0067E-04	7.4446E-04
S-32	16032		4.4046E-05	9.7245E-05	1.7333E-04
S-33	16033		3.4777E-07	7.6781E-07	1.3685E-06
S-34	16034		1.9707E-06	4.3509E-06	7.7548E-06
S-36	16036		4.6369E-09	1.0237E-08	1.8247E-08
Br-79	35079		1.1294E-07	3.3578E-06	5.2199E-06
Br-81	35081		1.0987E-07	3.2664E-06	5.0778E-06
C-12	6012		6.5533E-07	9.5321E-06	5.9576E-09
C-13	6013		7.0879E-09	1.0310E-07	6.4435E-11

18 November 2019

Table A1-4. Atom densities of elements making up the brine and plutonium mixture.

Isotopes	ZAID	Water atom/b*cm	Culebra atom/b*cm	Castile atom/b*cm	Salado atom/b*cm
H-1	1001	6.6606E-01	6.6453E-02	6.0433E-02	5.9081E-02
H-2	1002	7.6605E-05	7.6430E-06	6.9506E-06	6.7951E-06
O-16	8016	3.3307E-01	3.3417E-02	3.0644E-02	3.0277E-02
Na-23	11023		3.6033E-04	2.8681E-03	2.4876E-03
Mg-24	12024		9.9620E-06	8.8389E-06	3.0120E-04
Mg-25	12025		1.2612E-06	1.1190E-06	3.8131E-05
Mg-26	12026		1.3886E-06	1.2320E-06	4.1982E-05
K-39	19039		4.6486E-06	5.3276E-05	1.9756E-04
K-40	19040		5.8320E-10	6.6839E-09	2.4785E-08
K-41	19041		3.3548E-07	3.8448E-06	1.4257E-05
Ca-40	20040		1.3390E-05	6.8511E-06	4.5062E-06
Ca-42	20042		8.9369E-08	4.5725E-08	3.0075E-08
Ca-43	20043		1.8647E-08	9.5408E-09	6.2753E-09
Ca-44	20044		2.8814E-07	1.4742E-07	9.6964E-08
Ca-46	20046		5.5251E-10	2.8269E-10	1.8593E-10
Ca-48	20048		2.5830E-08	1.3216E-08	8.6924E-09
B-10	5010		3.3463E-07	7.3835E-06	1.7344E-05
B-11	5011		1.3469E-06	2.9720E-05	6.9812E-05
Cl-35	17035		2.5798E-04	2.1417E-03	2.3386E-03
Cl-37	17037		8.2541E-05	6.8524E-04	7.4824E-04
S-32	16032		4.3926E-05	9.5104E-05	1.7420E-04
S-33	16033		3.4682E-07	7.5090E-07	1.3754E-06
S-34	16034		1.9653E-06	4.2551E-06	7.7941E-06
S-36	16036		4.6243E-09	1.0012E-08	1.8339E-08
Br-79	35079		1.1264E-07	3.2839E-06	5.2463E-06
Br-81	35081		1.0957E-07	3.1945E-06	5.1035E-06
C-12	6012		6.5355E-07	9.3222E-06	5.9878E-09
C-13	6013		7.0686E-09	1.0083E-07	6.4762E-11
Pu-239	94239	8.0257E-04	1.3632E-04	3.9894E-04	4.7585E-04

Table A2-1. MCNP computed k^{eff} values compared to SCALE criticality S-curves for minimum Pu mass in WIPP brines and goethite

	SCALE			MCNP					
Brine	Mass Min (kg)	Radius Min (m)	Conc at Min Mass (kg/m³)	Mass Min (kg)	Radius Min (m)	Conc at Min Mass (kg/m³)	k_{eff}	+/- error	M:F Ratio
Water	N/A	N/A	N/A	2.978384	0.217599	79.0115	1.00005	0.00028	194.0895
Castile	N/A	N/A	N/A	4.33048	0.226300	89.2060	1.00003	0.00027	144.6377
Salado	N/A	N/A	N/A	4.814749	0.22605	99.511	1.00002	0.00028	128.647

*N/A means that the numbers have not yet been generated.

Table A2-2. MCNP computed asymptote values compared to SCALE criticality S-curves for Pu in WIPP brines and goethite

Brine	SCALE	MCNP
	Minimum kg/m³	Minimum kg/m³
Water	N/A	18.545
Castile	N/A	24.719
Salado	N/A	26.7900

*N/A means that the numbers have not yet been generated.

18 November 2019

Table A2-3. Atom densities of elements making up the brine and goethite.

Isotopes	ZAID	Water atom/b*cm	Castile atom/b*cm	Salado atom/b*cm
H-1	1001	3.3971E-02	3.2774E-02	3.2546E-02
H-2	1002	3.9072E-06	3.7694E-06	3.7432E-06
O-16	8016	4.7894E-02	4.7382E-02	4.7327E-02
Na-23	11023		5.8656E-04	4.9502E-04
Mg-24	12024		1.8076E-06	5.9937E-05
Mg-25	12025		2.2884E-07	7.5879E-06
Mg-26	12026		2.5195E-07	8.3543E-06
K-39	19039		1.0895E-05	3.9313E-05
K-40	19040		1.3669E-09	4.9321E-09
K-41	19041		7.8629E-07	2.8371E-06
Ca-40	20040		1.4011E-06	8.9671E-07
Ca-42	20042		9.3512E-09	5.9848E-09
Ca-43	20043		1.9512E-09	1.2488E-09
Ca-44	20044		3.0149E-08	1.9296E-08
Ca-46	20046		5.7813E-11	3.7000E-11
Ca-48	20048		2.7027E-09	1.7298E-09
B-10	5010		1.5100E-06	3.4514E-06
B-11	5011		6.0779E-06	1.3892E-05
Cl-35	17035		4.3799E-04	4.6536E-04
Cl-37	17037		1.4014E-04	1.4890E-04
S-32	16032		1.9449E-05	3.4666E-05
S-33	16033		1.5356E-07	2.7371E-07
S-34	16034		8.7020E-07	1.5510E-06
S-36	16036		2.0475E-09	3.6494E-09
Br-79	35079		6.7158E-07	1.0440E-06
Br-81	35081		6.5329E-07	1.0156E-06
C-12	6012		1.9065E-06	1.1915E-09
C-13	6013		2.0620E-08	1.2887E-11
Fe-54	26054	1.2043E-03	1.2043E-03	1.2043E-03
Fe-56	26056	1.8905E-02	1.8905E-02	1.8905E-02
Fe-57	26057	4.3661E-04	4.3661E-04	4.3661E-04
Fe-58	26058	5.8104E-05	5.8104E-05	5.8104E-05

18 November 2019

Table A2-4. Atom densities of elements making up the brine, goethite, and plutonium mixture at minimum mass

Isotopes	ZAID	Water atom/b*cm	Castile atom/b*cm	Salado atom/b*cm
H-1	1001	3.3739E-02	3.2500E-02	3.2246E-02
H-2	1002	3.8804E-06	3.7379E-06	3.7088E-06
O-16	8016	4.7778E-02	4.7243E-02	4.7174E-02
Na-23	11023		5.7337E-04	4.8261E-04
Mg-24	12024		1.7670E-06	5.8434E-05
Mg-25	12025		2.2370E-07	7.3976E-06
Mg-26	12026		2.4629E-07	8.1448E-06
K-39	19039		1.0650E-05	3.8327E-05
K-40	19040		1.3362E-09	4.8084E-09
K-41	19041		7.6861E-07	2.7660E-06
Ca-40	20040		1.3696E-06	8.7422E-07
Ca-42	20042		9.1410E-09	5.8347E-09
Ca-43	20043		1.9073E-09	1.2174E-09
Ca-44	20044		2.9471E-08	1.8812E-08
Ca-46	20046		5.6513E-11	3.6072E-11
Ca-48	20048		2.6420E-09	1.6864E-09
B-10	5010		1.4760E-06	3.3649E-06
B-11	5011		5.9413E-06	1.3544E-05
Cl-35	17035		4.2814E-04	4.5369E-04
Cl-37	17037		1.3699E-04	1.4516E-04
S-32	16032		1.9012E-05	3.3796E-05
S-33	16033		1.5011E-07	2.6684E-07
S-34	16034		8.5064E-07	1.5121E-06
S-36	16036		2.0015E-09	3.5579E-09
Br-79	35079		6.5648E-07	1.0178E-06
Br-81	35081		6.3861E-07	9.9011E-07
C-12	6012		1.8636E-06	1.1617E-09
C-13	6013		2.0156E-08	1.2564E-11
Fe-54	26054	1.2043E-03	1.2043E-03	1.2043E-03
Fe-56	26056	1.8905E-02	1.8905E-02	1.8905E-02
Fe-57	26057	4.3661E-04	4.3661E-04	4.3661E-04
Fe-58	26058	5.8104E-05	5.8104E-05	5.8104E-05
Pu-239	94239	1.7385E-04	2.2473E-04	2.5069E-04

18 November 2019

Table A3-1. MCNP computed k^{eff} values compared to SCAL criticality S-curves for Pu minimum mass in WIPP brines and Culebra Dolomite

	SCALE			MCNP					
Brine	Mass Min (kg)	Radius Min (m)	Conc at Min Mass (kg/m³)	Mass Min (kg)	Radius Min (m)	Conc at Min Mass (kg/m³)	k_{eff}	+/- error	M:F Ratio
Water	1.6056	0.29380	15.114	1.812987	0.31380	14.007	1.00002	0.00027	378.9366
Culebra	2.0745	0.32000	15.114	2.325151	0.33240	15.114	0.99994	0.00028	347.4526
Castile	3.2348	0.24465	52.738	7.4765	0.371777	34.7348	0.99992	0.00028	136.7272
Salado	6.0907	0.30210	52.738	9.672852	0.379585	42.222	0.99999	0.00027	109.96

*PuO_2 was used in these calculations.

Table I3-2. MCNP computed asymptote values compared to SCALE criticality S-curves for Pu in WIPP brines and Culebra Dolomite

	SCALE	MCNP
Brine	Minimum kg/m³	Minimum kg/m³
Water	3.0635	2.891
Culebra	3.7260	3.6789
Castile	14.280	9.7750
Salado	13.94	11.9165

*PuO_2 was used in these calculations.

18 November 2019

Table A3‑3. Atom densities of elements making up the WIPP brine and Culebra Dolomite.

		Water	Culebra	Castile	Salado
Isotope	ZAID	atom/b*cm	atom/b*cm	atom/b*cm	atom/b*cm
H-1	1001	1.3370E-02	1.3327E-02	1.2172E-02	1.1695E-02
H-2	1002	1.5377E-06	1.5328E-06	1.3999E-06	1.3450E-06
O-16	8016	5.1140E-02	5.1156E-02	5.0628E-02	5.0658E-02
Na-23	11023	4.4307E-05	1.1657E-04	6.3086E-04	5.2899E-04
Mg-24	12024	5.6725E-03	5.6745E-03	5.6743E-03	5.7312E-03
Mg-25	12025	7.1813E-04	7.1838E-04	7.1836E-04	7.2556E-04
Mg-26	12026	7.9066E-04	7.9094E-04	7.9091E-04	7.9884E-04
K-39	19039	2.4469E-05	2.5401E-05	3.5364E-05	6.2961E-05
K-40	19040	3.0698E-09	3.1868E-09	4.4367E-09	7.8989E-09
K-41	19041	1.7659E-06	1.8331E-06	2.5521E-06	4.5437E-06
Ca-40	20040	6.9760E-03	6.9787E-03	6.9774E-03	6.9769E-03
Ca-42	20042	4.6559E-05	4.6577E-05	4.6568E-05	4.6565E-05
Ca-43	20043	9.7147E-06	9.7185E-06	9.7167E-06	9.7160E-06
Ca-44	20044	1.5011E-04	1.5017E-04	1.5014E-04	1.5013E-04
Ca-46	20046	2.8784E-07	2.8796E-07	2.8790E-07	2.8788E-07
Ca-48	20048	1.3457E-05	1.3462E-05	1.3459E-05	1.3458E-05
B-10	5010		6.7111E-08	1.5100E-06	3.3793E-06
B-11	5011		2.7013E-07	6.0779E-06	1.3602E-05
Cl-35	17035		5.1737E-05	4.3799E-04	4.5564E-04
Cl-37	17037		1.6554E-05	1.4014E-04	1.4579E-04
S-32	16032	5.3758E-04	5.4639E-04	5.5703E-04	5.7152E-04
S-33	16033	4.2445E-06	4.3141E-06	4.3981E-06	4.5125E-06
S-34	16034	2.4052E-05	2.4446E-05	2.4922E-05	2.5571E-05
S-36	16036	5.6594E-08	5.7521E-08	5.8641E-08	6.0167E-08
Br-79	35079		2.2589E-08	6.7158E-07	1.0222E-06
Br-81	35081		2.1974E-08	6.5329E-07	9.9436E-07
C-12	6012	1.3590E-02	1.3590E-02	1.3592E-02	1.3590E-02
C-13	6013	1.4698E-04	1.4699E-04	1.4701E-04	1.4698E-04
Fe-54	26054	2.2113E-06	2.2113E-06	2.2113E-06	2.2113E-06
Fe-56	26056	3.4713E-05	3.4713E-05	3.4713E-05	3.4713E-05
Fe-57	26057	8.0167E-07	8.0167E-07	8.0167E-07	8.0167E-07
Fe-58	26058	1.0669E-07	1.0669E-07	1.0669E-07	1.0669E-07
Si-28	14028	3.2666E-04	3.2666E-04	3.2666E-04	3.2666E-04
Si-29	14029	1.6595E-05	1.6595E-05	1.6595E-05	1.6595E-05
Si-30	14030	1.0952E-05	1.0952E-05	1.0952E-05	1.0952E-05
Al-27	13027	7.0025E-05	7.0025E-05	7.0025E-05	7.0025E-05

18 November 2019

Table A3-4. Atom densities of elements making up the WIPP brine, Culebra Dolomite, and plutonium mixture.

Isotope	ZAID	Water atom/b*cm	Culebra atom/b*cm	Castile atom/b*cm	Salado atom/b*cm
H-1	1001	1.3370E-02	1.3228E-02	1.1963E-02	1.1695E-02
H-2	1002	1.5377E-06	1.5214E-06	1.3759E-06	1.3450E-06
O-16	8016	5.1211E-02	5.1182E-02	5.0697E-02	5.0658E-02
Na-23	11023	4.4307E-05	1.1603E-04	6.2078E-04	5.2899E-04
Mg-24	12024	5.6725E-03	5.6745E-03	5.6743E-03	5.7312E-03
Mg-25	12025	7.1813E-04	7.1838E-04	7.1836E-04	7.2556E-04
Mg-26	12026	7.9066E-04	7.9094E-04	7.9091E-04	7.9884E-04
K-39	19039	2.4469E-05	2.5394E-05	3.5177E-05	6.2961E-05
K-40	19040	3.0698E-09	3.1859E-09	4.4132E-09	7.8989E-09
K-41	19041	1.7659E-06	1.8326E-06	2.5386E-06	4.5437E-06
Ca-40	20040	6.9760E-03	6.9786E-03	6.9774E-03	6.9769E-03
Ca-42	20042	4.6559E-05	4.6577E-05	4.6568E-05	4.6565E-05
Ca-43	20043	9.7147E-06	9.7185E-06	9.7167E-06	9.7160E-06
Ca-44	20044	1.5011E-04	1.5017E-04	1.5014E-04	1.5013E-04
Ca-46	20046	2.8784E-07	2.8795E-07	2.8790E-07	2.8788E-07
Ca-48	20048	1.3457E-05	1.3462E-05	1.3459E-05	1.3458E-05
B-10	5010		6.6609E-08	1.4840E-06	3.3793E-06
B-11	5011		2.6811E-07	5.9735E-06	1.3602E-05
Cl-35	17035		5.1350E-05	4.3046E-04	4.5564E-04
Cl-37	17037		1.6430E-05	1.3773E-04	1.4579E-04
S-32	16032	5.3758E-04	5.4633E-04	5.5670E-04	5.7152E-04
S-33	16033	4.2445E-06	4.3136E-06	4.3954E-06	4.5125E-06
S-34	16034	2.4052E-05	2.4443E-05	2.4907E-05	2.5571E-05
S-36	16036	5.6594E-08	5.7514E-08	5.8606E-08	6.0167E-08
Br-79	35079		2.2421E-08	6.6004E-07	1.0222E-06
Br-81	35081		2.1810E-08	6.4207E-07	9.9436E-07
C-12	6012	1.3590E-02	1.3590E-02	1.3592E-02	1.3590E-02
C-13	6013	1.4698E-04	1.4699E-04	1.4700E-04	1.4698E-04
Fe-54	26054	2.2113E-06	2.2113E-06	2.2113E-06	2.2113E-06
Fe-56	26056	3.4713E-05	3.4713E-05	3.4713E-05	3.4713E-05
Fe-57	26057	8.0167E-07	8.0167E-07	8.0167E-07	8.0167E-07
Fe-58	26058	1.0669E-07	1.0669E-07	1.0669E-07	1.0669E-07
Si-28	14028	3.2666E-04	3.2666E-04	3.2666E-04	3.2666E-04
Si-29	14029	1.6595E-05	1.6595E-05	1.6595E-05	1.6595E-05
Si-30	14030	1.0952E-05	1.0952E-05	1.0952E-05	1.0952E-05
Al-27	13027	7.0025E-05	7.0025E-05	7.0025E-05	7.0025E-05
Pu-239	94239	3.5286E-05	3.8075E-05	8.7503E-05	1.0636E-04

Table A4-1. MCNP computed k^{eff} values compared to SCALE criticality S-curves for minimum Pu mass in WIPP brines and NRC concrete

Brine	SCALE			MCNP					
	Mass Min (kg)	Radius Min (m)	Conc at Min Mass (kg/m³)	Mass Min (kg)	Radius Min (m)	Conc at Min Mass (kg/m³)	k_{eff}	+/- error	M:F Ratio
Water	1.5296	0.2854	15.708	2.389	0.344086	14	0.99990	0.00026	499.41
Salado	6.4677	0.3156	49.119	5.95	0.306289	49.119	0.99995	0.00028	185.41

*PuO$_2$ was used in these calculations.

Table I4-2. MCNP computed asymptote values compared to SCALE criticality S-curves for Pu in WIPP brines and NRC Concrete

Brine	SCALE	MCNP
	Minimum kg/m³	Minimum kg/m³
Water	~4	3.354
Salado	13.184	13.318

*PuO$_2$ was used in these calculations.

Table A4-3. Atom densities of elements making up WIPP brine with NRC concrete.

Isotopes	ZAID	Water atoms/b*cm	Salado atoms/b*cm
Si28	14028	1.22609E-02	1.22609E-02
Si-29	14029	6.22863E-04	6.22863E-04
Si-30	14030	4.11076E-04	4.11076E-04
Ca-40	20040	1.17997E-03	1.18086E-03
Ca-42	20042	7.87528E-06	7.88126E-06
Ca-43	20043	1.64322E-06	1.64447E-06
Ca-44	20044	2.53908E-05	2.54101E-05
Ca-46	20046	4.86880E-08	4.87250E-08
Ca-48	20048	2.27616E-06	2.27789E-06
Al-27	13027	1.39540E-03	1.39540E-03
Fe-54	26054	1.62233E-05	1.62233E-05
Fe-56	26056	2.54672E-04	2.54672E-04
Fe-57	26057	5.88148E-06	5.88148E-06
Fe-58	26058	7.82718E-07	7.82718E-07
Na-23	11023	1.39808E-03	1.89310E-03
H-1	1001	1.76154E-02	2.29403E-02
H-2	1002	2.02600E-06	2.63843E-06
O-16	8016	3.98240E-02	4.26328E-02
Mg-24	12024		5.99368E-05
Mg-25	12025		7.58790E-06
Mg26	12026		8.35428E-06
K-39	19039		3.93129E-05
K-40	19040		4.93213E-09
K-41	19041		2.83712E-06
B-10	5010		3.45141E-06
B-11	5011		1.38924E-05
Cl-35	17035		4.65362E-04
Cl-37	17037		1.48896E-04
S-32	16032		3.46658E-05
S-33	16033		2.73706E-07
S-34	16034		1.55100E-06
S-36	16036		3.64942E-09
Br-79	35079		1.04400E-06
Br-81	35081		1.01558E-06
C-12	6012		1.19154E-09
C-13	6013		1.28874E-11

18 November 2019

Table A4-4. Atom densities of elements making up the WIPP brine and plutonium mixture with NRC concrete.

Isotopes	ZAID	Water atoms/b*cm	Salado atoms/b*cm
Si28	14028	1.22609E-02	1.22609E-02
Si-29	14029	6.22863E-04	6.22863E-04
Si-30	14030	4.11076E-04	4.11076E-04
Ca-40	20040	1.17997E-03	1.18086E-03
Ca-42	20042	7.87528E-06	7.88126E-06
Ca-43	20043	1.64322E-06	1.64447E-06
Ca-44	20044	2.53908E-05	2.54101E-05
Ca-46	20046	4.86880E-08	4.87250E-08
Ca-48	20048	2.27616E-06	2.27789E-06
Al-27	13027	1.39540E-03	1.39540E-03
Fe-54	26054	1.62233E-05	1.62233E-05
Fe-56	26056	2.54672E-04	2.54672E-04
Fe-57	26057	5.88148E-06	5.88148E-06
Fe-58	26058	7.82718E-07	7.82718E-07
Na-23	11023	1.39808E-03	1.89310E-03
H-1	1001	1.76154E-02	2.29403E-02
H-2	1002	2.02600E-06	2.63843E-06
O-16	8016	3.98946E-02	4.26328E-02
Mg-24	12024		5.99368E-05
Mg-25	12025		7.58790E-06
Mg26	12026		8.35428E-06
K-39	19039		3.93129E-05
K-40	19040		4.93213E-09
K-41	19041		2.83712E-06
B-10	5010		3.45141E-06
B-11	5011		1.38924E-05
Cl-35	17035		4.65362E-04
Cl-37	17037		1.48896E-04
S-32	16032		3.46658E-05
S-33	16033		2.73706E-07
S-34	16034		1.55100E-06
S-36	16036		3.64942E-09
Br-79	35079		1.04400E-06
Br-81	35081		1.01558E-06
C-12	6012		1.19154E-09
C-13	6013		1.28874E-11
Pu-239	94239	3.52761E-05	1.23739E-04

18 November 2019

Fissile Mass and Concentration Necessary in Geologic Media Near Bedded Salt Repository

Table A5-1. MCNP computed k^{eff} values compared to SCALE criticality S-curves for minimum Pu mass in Salado brine with NaCl

	SCALE			MCNP					
Brine	Mass Min (kg)	Radius Min (m)	Conc at Min Mass (kg/m³)	Mass Min (kg)	Radius Min (m)	Conc at Min Mass (kg/m³)	k_{eff}	+/- error	M:F Ratio
Salado	132.6210	.25000	2026.3	123.8	.2443296	2026.3	1.00003	0.00027	9.38E-03

*The H/X ratio is not calculated because the minimum mass for criticality occurs when the fissile fraction for PuO_2 is at unity.
*PuO_2 was used in these calculations.

Table A5-2. MCNP Computed Asymptote values compared to SCALE Criticality S-Curves for Pu in Salado brine and NaCl

	SCALE	MCNP
Brine	Minimum kg/m³	Minimum kg/m³
Salado	137.74	232.8

*PuO_2 was used in these calculations.

Table A5-3. Atom densities of elements making up the brine and NaCl mixture

Isotopes	ZAID	Salado Atoms/b*cm
H-1	1001	4.78759E-05
H-2	1002	5.50637E-09
O-16	8016	4.81787E-05
Na-23	11023	1.78924E-02
Mg-24	12024	4.88147E-07
Mg-25	12025	6.17986E-08
Mg-26	12026	6.80403E-08
K-39	19039	3.20179E-07
K-40	19040	4.01691E-11
K-41	19041	2.31065E-08
Ca-40	20040	1.50972E-04
Ca-42	20042	1.50987E-04
Ca-43	20043	1.50995E-04
Ca-44	20044	1.51002E-04
Ca-46	20046	1.51017E-04
Ca-48	20048	1.51033E-04
B-10	5010	2.81095E-08
B-11	5011	1.13144E-07
Cl-35	17035	1.35560E-02
Cl-37	17037	4.33734E-03
S-32	16032	2.82331E-07
S-33	16033	2.22916E-09
S-34	16034	1.26319E-08
S-36	16036	2.97222E-11
Br-79	35079	8.50269E-09
Br-81	35081	8.27121E-09
C-12	6012	9.70434E-12
C-13	6013	1.04960E-13

Table A5-4. Atom densities of plutonium with NaCl. The minimum mass occurs when the fissile fraction in the pores is unity.

Isotopes	ZAID	Salado Atoms/b*cm
H-1	1001	4.78759E-05
H-2	1002	5.50637E-09
O-16	8016	1.02574E-02
Na-23	11023	1.78924E-02
Mg-24	12024	4.88147E-07
Mg-25	12025	6.17986E-08
Mg-26	12026	6.80403E-08
K-39	19039	3.20179E-07
K-40	19040	4.01691E-11
K-41	19041	2.31065E-08
Ca-40	20040	1.50972E-04
Ca-42	20042	1.50987E-04
Ca-43	20043	1.50995E-04
Ca-44	20044	1.51002E-04
Ca-46	20046	1.51017E-04
Ca-48	20048	1.51033E-04
B-10	5010	2.81095E-08
B-11	5011	1.13144E-07
Cl-35	17035	1.35560E-02
Cl-37	17037	4.33734E-03
S-32	16032	2.82331E-07
S-33	16033	2.22916E-09
S-34	16034	1.26319E-08
S-36	16036	2.97222E-11
Br-79	35079	8.50269E-09
Br-81	35081	8.27121E-09
C-12	6012	9.70434E-12
C-13	6013	1.04960E-13
Pu-239	94239	5.10460E-03

18 November 2019

Table A6-1. MCNP computed k^{eff} values compared to SCAL criticality S-Curves for minimum 5% enriched uranium mass in water

	SCALE			MCNP				
Brine	Mass Min (kg)	Radius Min (m)	Conc at Min Mass (kg/m³)	Mass Min (kg)	Radius Min (m)	Conc at Min Mass (kg/m³)	k_{eff}	+/- error
Water	36.141	.204	1016.3	31.95	.19246	1070	.99990	0.00027

*Uranium that was 5% enriched was used in these calculations.

Table A6-3. Atom densities of elements making up water

		Water
Isotope	ZAID	atom/b*cm
H-1	1001	6.6648E-02
H2	1002	7.6654E-06
O-16	8016	3.3328E-02

Table A6-4. Atom densities of elements making up the water and 5% enriched uranium mixture

		Water
Isotope	ZAID	atom/b*cm
H-1	1001	6.6648E-02
H2	1002	7.6654E-06
O-16	8016	3.3328E-02
U-235	92235	1.3707E-04
U-238	92238	2.5715E-03

18 November 2019

Table A7-1. MCNP computed k^{eff} values compared to SCALE criticality S-curves for 15% enriched uranium in water

	SCALE			MCNP				
Brine	Mass Min (kg)	Radius Min (m)	Conc at Min Mass (kg/m³)	Mass Min (kg)	Radius Min (m)	Conc at Min Mass (kg/m³)	k_{eff}	+/- error
Water	~9	~.19	~320	7.184	.16526	380	.99997	0.00027

*Uranium that was 15% enriched was used in these calculations.

Table I7-3. Atom densities of elements making up water

		Water
Isotope	ZAID	atom/b*cm
H-1	1001	6.6648E-02
H2	1002	7.6654E-06
O-16	8016	3.3328E-02

Table A7-4. Atom densities of elements making up water and 15% enriched uranium mixture

		Water
Isotope	ZAID	atom/b*cm
H-1	1001	6.6648E-02
H2	1002	7.6654E-06
O-16	8016	3.3328E-02
U-235	92235	1.4604E-04
U-238	92238	8.1710E-04

18 November 2019